POLITECNICO
MILANO 1863

SCUOLA DI INGEGNERIA INDUSTRIALE
E DELL'INFORMAZIONE

CubeSat's payload and orbit selection for in-situ debris characterisation

Tesi di Laurea Magistrale in
Space Engineering - Ingegneria Spaziale

Author: **Davide Andi**

Student ID: 962755
Advisor: Prof.ssa Camilla Colombo
Co-advisors: Mr. Andrea Muciaccia
Academic Year: 2022-23

Abstract

Space sustainability is one of the major concern for the future of space activities. Years of unregulated activities have lead to an uncontrolled growth of the space debris, and an increase of the risk for spacecraft. For this reason it is important to characterise the space debris environment, increasing the accuracy of the models, and developing suitable end-of-life solutions. This thesis present a preliminary payload selection for a CubeSat mission to characterise the debris environment in the LEO orbit. Firstly will be selected the operational orbit. Using the MASTER 8 software will be performed a flux and impact analysis to identify the orbits that could satisfied the mission requirements; than a natural decay analysis is performed to select an orbit compliant with a natural re-entry in 25 years. In the second part will be selected a suitable payload based on a literature review. Finally a first sizing of the payload will be performed.

Keywords: CubeSat, Space Debris, Space Environment, LEO, PVDF

Sommario

La sostenibilità spaziale è una delle maggiori preoccupazioni per il futuro delle attività spaziali. Anni di sfruttamento hanno portato ad una crescita incotrollata dei detriti, causando un aumento dei rischi per i satelliti. Per questo motivo è importante studiare e caratterizzare il fenomeno dei detriti spaziali, aumentando la precisione dei modelli, e sviluppando specifiche strategie di fine vita dei satelliti. Questa tesi mira a presentare una prima selezione di uno strumento per una missione CubeSat volta a definire l'ambiente dei detriti nella bassa orbita terrestre. Come prima cosa è stata selezionata un orbita nominale. Usando il software MASTER 8 è stata effettuata una analisi sul numero di impatti previsti e sul flusso di detriti, per identificare le orbite che soddisfino i requisiti della missione; inoltre è stata fatta una analisi sul naturale decadimento del satellite, per identificare un orbita che sia compatibile con un rientro in 25 anni in caso di problemi. Successivamente basandosi su una ricerca storica, viene identificato uno strumento ottimale per la missione. In fine vengono definite, in prima approssimazione, le caratteristiche dello strumento scelto.

Parole chiave: CubeSat, Detriti Spaziali, Ambiente Spaziale, LEO, PVDF

Acknowledgements

First i would like to express my gratitude to my supervisor, Prof.ssa Camilla Colombo, for the opportunity to work on this topic, and her guidance. I am also grateful to my co-supervisor, Mr. Andrea Muciaccia, for the precious advices and constant support that he gave me.

<center>**********</center>

Special thanks goes to my parents, Graziella and Marco, for their willingness, help and sacrifice that allows me to get here. Thanks to my sister Elisa, and my brother-in-law Paolo, who always encouraged me to give more, and do my best. Finally thanks to all my family, that supported me.

In the end i would like to thanks all my friends. The guys encountered at Politecnico with whom i shared the last six years. They have made lessons more pleasant, and help me a lot. Thanks to the fellows from the basket team, that helps me relived the stress; and thank you to the "Nakama" from the Regimosky and the community of OnepieceGT, whom with i share a great passion.

Finally, thanks to all the people encountered, that in their own way have contributed to forming me.

<center>Thank You All</center>

Contents

List of Figures

List of Tables

Acronyms

Acronym	Description
AIDA	Advance Impact Detector Assembly
CAM	Collision Avoidance Manoeuvre
CDA	Cosmic Dust Analyzer
CIDA	Cometary and Interstellar Dust Analyzer
CIRA	COSPAR International Reference Atmosphere
CNES	Centre national d'études spatiales
DART	Double Asteroid Redirection Test
DCU	central Control unit
DDS	Dust Detector System
DEBIE	DEBris In-orbit Evaluator
DFMI	Dust Flux Monitor Instrument
DID	Dust Impact Detector
DPU	Data Processing Unit
DRAGONS	Debris Resistive/Acoustic Grid Orbital Navy-NASA Sensor
EOL	End of Life
ESA	European Space Agency
GDS	Grain Detection System
GEO	Geostationary Earth Orbit
GIADA	Grain Impact Analyzer and dust Accumulator
HVI	Hypervelocity Impact
IADC	Inter Agency Space Debris Coordination Committee
IMEX	Interplanetary Meteoroid environment for EXploration model
IS	Impact Sensor
ISS	International Space Station
JAXA	Japan Aerospace eXploration Agency

Acronym	Description
LDEF	Long Duration Exposure Facility
LEO	Low Earth Orbit
MDA	Micrometeoroid Detector and Analyzer
MDM	Mercury Dust Monitor
MDU	Main Detector Unit
MTBG	BackGround Meteoroids
NASA	National Aeronautics and Space Administration
NOAA	National Oceanic and Atmospheric Administration
ODPO	Orbital Debris Program Office
PDD	Particle Detection Device
PDD	Piezoelectric Dust Detector
PVDF	Polyvinylidene Fluoride
PZT	(piezoelectric) Lead Zirconate Titanate
RAAN	Right Ascension of Ascending Node
s/c	Spacecraft
SDC	Student Dust Counter
SDM	Space Debris Monitor
SDU	Secondary Detector Unit
SEU	Single Event Upsets
SPADUS	SPAce DUSt experiment
SSO	Sun Synchronous Orbit
SSN	Space Surveillance Network
SU	Sensor Unit
ToF	Time of Flight
USSA76	U.S. Standard Atmosphere 1976
VISTA	Volatile In-Situ Thermogravimetre Analyser

List of Symbols

Variable	Description	Units
μ	Earth Gravitational Constant	km^3/s^2
ρ	Density	kg/m^3
Φ	Latitude	deg
A_C	Cross Sectional Area	m^2
A_m	Area to mass ratio	m^2/kg
r	s/c Position vector [x ; y; z]	km
C_D	Drag Coefficient	[-]
F	Solar Radio Flux at 10.7 cm	sfu
m	mass	kg
P_k	Lagendre polynomials	[-]
R	Equatorial Radius	km
T_{EXO}	Exospheric Temperature	K
v_{rel}	relative velocity (s/c to atm)	km/s

Introduction

At the beginning of space exploration, no guidelines or regulations had been developed to limit the impact of space activities on space environment. All the attention was focused on the technology development. Earth's orbit capacity have been treated as an infinite resource, and no end-of-life disposal strategies were implemented. During the last decade the number of launches has increased deeply, thanks to the reduced costs of launching new satellites in orbit [26]. Better regulations and a deeper understanding of the sustainable use of the space environment are needed to face this increment [11]. Since 1993, the Inter Agency Space Debris Coordination Committee (IADC) [46] introduces the recommended guidelines for the end-of-life mitigation strategies. If no action will be taken in this direction, in the future a saturation of the orbits capability and an unregulated growth of untraceable space debris will lead to a more difficult access to space.

Background

Since the launch of Sputnik in 1957, about 15760 satellite have been placed in Earth orbit, 10550 of which still in space, but only 8400 still functioning [25]; the rest are inactive, orbiting without control, and representing a threat to operational spacecraft.
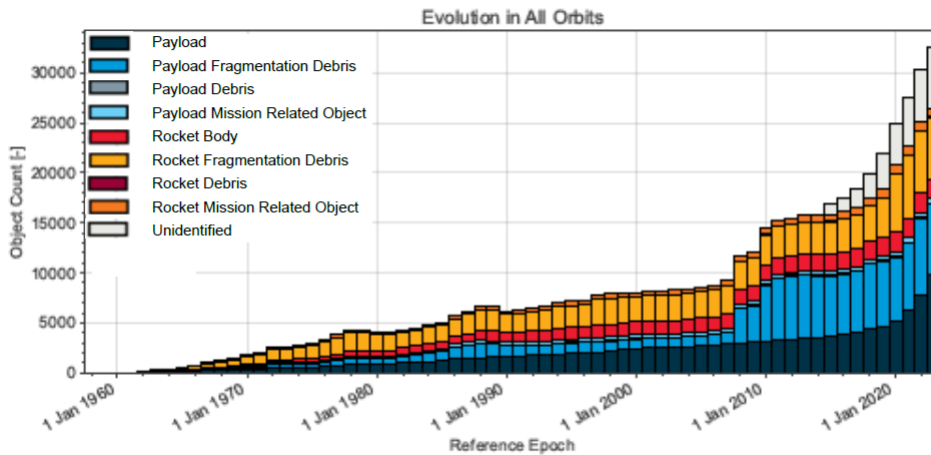

Figure 1: Evolution of space objects population by object class. Credit: ESA [26]

Figure 1 represent the time evolution of space objects, divided by class. Other than payloads, most of the mission-related objects and rocket bodies remain in orbit for long time, representing an additional hazard. However, the largest part of the space population is represented by satellite breakup debris, defined as fragments of other objects generated by destructive dissociation, collisions and explosions of orbital payload, rocket body, or structure. The Unidentified class represent all the objects impossible to be identified and tracked.

Due to the high impact velocity in LEO (up to 20 km/s), collision with impactors larger than 1 cm could disable operative spacecraft, and debris larger than 10 cm could lead to catastrophic events : complete satellite destruction and generation of a debris cloud [37]. The main issue is related to the Kessler Syndrome [36], where there is a continuous growth of debris population due to concatenated collisions and explosions. The theory stressed that, over a long time period, the debris flux will increase exponentially, controlled by random collisions, even if a zero input rate is maintained [36]. For this reason the collision avoidance has began to be part of the spacecraft's routine operations.

Among the impactors a further distinction can be made between untraceable and traceable objects. The US Space Surveillance Network (SSN), using ground-based radars and optical measurements, can track objects larger than 5 cm in LEO and larger than 1 m in GEO [48], allowing to plan collision avoidance manoeuvres to avoid catastrophic event. Smaller objects, instead, cannot be tracked and must be estimated or modelled in a different way, based on in-situ observations and statistical analysis. In fact, also millimeter and sub-millimeter particles could cause local damage, or degrade the satellite performance. In light of this situation, all major space agencies agreed to work on the definition of mission guidelines and collision avoidance whose goal is to limit the debris proliferation. The first important concept is to consider the space environment as a shared and limited natural resource. General aim is to reduce the growth of space debris by ensuring that satellite and orbital stages are designed, operated, and disposed in a way that avoid the generation of debris through their lifetime. During operations debris should not be released intentionally. It is also important to remove spacecraft and launch vehicle from protected regions at the end of the mission, performing atmospheric re-entry or placing them in graveyard orbits. In the former case it is also important to avoid any harm to Earth's environment and population. In addition, for LEO missions, the current procedure provides that the re-entry phase has to be successfully completed in a maximum of 25 years [26].

Future of space operations depends on the compliance to these guidelines. Unregulated space activities would lead to an uncontrolled increase of space debris and a dangerous environment. The knowledge of a debris models is important to design satellite that can

withstand impacts from small objects, and design collision avoidance system. Furthermore, it can also be a tool to predict the future evolution of the debris orbit environment, making possible to perform more in-depth analysis suited to improve the safety of future missions, and in general of the entire space around Earth.

e.Cube Mission

In this optics, the e.Cube mission aims at contributing to the technology and methodology advancement for space debris mitigation. Its scientific objectives are :

1. Increase spacecraft autonomy in performing CAMs;

2. Support the space debris modelling with in-orbit collection of data of non-trackable particles;

3. Characterise the atmosphere for more accurate re-entry predictions as well as the thermomechanical loads experienced during re-entry phase.

The mission consists in a 12U CubeSat deployed in LEO orbit where the operational phase will be dedicated to three experiments. First, the autonomous CAM experiment will perform several CAM tests for simulated close approaches with a virtual debris. Next, a Particle Detection Device (PDD), in the frontal side of the spacecraft, will collect data over one year on the highest possible amount of sub-millimetre particles to validate the statistical distributions of non-trackable object in-use. Finally, an EOL manoeuvre for a quick re-entry will be implemented to collect in-situ measurements, in particular temperature and pressure, to characterize the thermosphere in the region below 200 km. The data and result of the e.Cube mission will be used to validate tools and technique currently used by the community, like long-term evolution models for space debris, re-entry prediction, and autonomous CAM for future traffic management [6].

The project, with a preliminary design, has been presented by C. Colombo et al. [5] at the 8th European Conference on Space Debris (virtual) at Darmastadt. The mission concept of operation and architecture, with a preliminary design focused on mission analysis and attitude control, has been analysed by M.P. Brenna [2]. A complete attitude analysis, focused on the atmospheric re-entry, has been analysed by F. Scala et al. [65], and presented at the 16th International Conference on Space Operations at Cape Town.

Thesi Objective

This thesis aims at presenting the preliminary design solution for the debris analysis phase of a CubeSat mission. The thesis resume the concept proposed by M.P. Brenna [2], in terms of flux and impacts analysis, and will introduce a complete natural decay simulation, compatible with the regulations. It will analyse a set of operational orbit, and will propose a different final solution based on a trade-off between flux/impacts data and the decay analysis. Than, a preliminary choice for the debris detection payload will be proposed, based on a literature review of different detection methods and sensors. A preliminary sizing will also be proposed.

The main objective of the thesis, is to find a solution for the in-situ debris detection, compatible with the CubeSat format. The LEO environment characterisation, done by the debris detection payload, could provide high fidelity models of the small space debris distribution. CubeSats could be a cost efficient way to perform this tasks, being able to access space frequently and at low costs, using piggyback launch opportunities. They could be efficient way to validate and expand the debris models currently available.

Thesis Organization

This thesis presents the preliminary design of the debris detection phase for a CubeSat mission. An overview of past mission, involved in this topic, is presented in the state of art (chapter 1). In chapter 2 the preliminary mission and payload requirement are collected. Chapter 3 present the selection of a suitable operational orbit for the debris data acquisition, compliant with the requirement. The choice will be based on the flux and impact analysis, based on MASTER data, and a complete natural decay simulation. Chapter 4 will analyse different payload options, analysing different detection methods and sensors combination. A final solution, with a preliminary sizing of the payload, will be proposed. Finally in chapter 5 the summaries of results, the conclusions and the main open points will be discussed.

1 | State of Art

In space there is a significant amount of small particle that comes from a variety of source, like interplanetary dust, interstellar dust, and man-made debris. Evaluate this flux can represent an important goal for scientific and engineering reasons. The former case allow to study the environment from a composition point of view, while the latter determine the hazard for space vehicles due to the impacts with these particles. Average debris impact speed in the LEO orbits can range from 5-20 km/s. Such impacts can be a significant problem for satellite, degrading its performance, and causing structural damages. It thus arises the need to define the particle population, characterising flux, impact time, size, speed, trajectory, ecc.

Over the last decades, many technologies have been developed for the detection and measurement of physical, chemical, and dynamical parameters of such particles. Passive and active instruments were initially used to study the cosmic dust in the Earth system and particles around other celestial body. Then, with the increase of the debris problem, they began to be used also for the characterisation of the Earth's debris environment and the validation of their statistical models.

1.1. Interplanetary Region

The characterisation of the interplanetary environment and the exploration of the Solar System has been one of the milestones of the space exploration. The study of different celestial body and their organisation can provides knowledge on the origin and evolution of Solar System. One of the main objective of this exploration is focused on the study of dust particles. Interstellar dust research start in 1930s, when astronomers realised the extinction of starlight in the interstellar medium. At that time information were only obtained by astronomical observation. It is only from the '70s, with the advent of on-board dust detectors, that the in-situ particle investigation became possible [38].

The first mission to explore the outer solar system and study the interplanetary dust particles, was Pioneer 10 [60]. Along its journey and its close passage to Jupiter, it has detected the flux of meteoroid impacts, of approximately $1 \times 10^{-9} g$, using pressure loss

detectors. A total of 67 impact were recorded between 1 and 5 AU, ten of which during the Jupiter encounter. The analysis of the retrieved data has reported an almost constant trend of the spatial density in this range, with one order of magnitude increase near Jupiter [34].

In 1974/75 Helios [58] characterise the interplanetary medium in the inner solar orbits up to 0.3 AU orbit. The purpose of the Micrometeoroid Detector and Analyzer was to investigate theories about the increase of particles toward the Sun and the dust density change near planets. The detection was done through an impact ionization detector, with a threshold of $1 \times 10^{-15}g$.

In 1985 the Giotto [57] mission set out to study the Comet P/Halley. One of the mission objective was to study the dust flux and their size/mass distribution using the Dust Impact Detector (DID). The entire meteoroid shield surface was used as impact target with a collection of transducers array to determine the impact momentum. Particle mass, density and ionisation were instead characterised by an impact plasma micro-perforation sensing array.

In the '90s three other missions reported data on interplanetary dust. The first to set out was Galileo [56], with the aim of studying the Jovian system. The Dust Detector System (DDS) was used to determine mass, impact velocity and charge state of individual particles. Its objectives were to measure the influence of Jupiter's gravitational field on interplanetary dust population. The instrument consisted of an impact ionization detector, a total of 115 impactors were identified. A similar instrument has flown also on Ulysses [24] in 1990. The mission aimed to explore the Sun's polar regions, focusing on solar wind, interplanetary magnetic field and complex wave and particles interaction inside the interplanetary medium. With more than 900 particles detected, it covered about 75% of one full 22-yr solar cycle and represent the biggest data set available. Finally, in 1997 the Cassini [51] spacecraft was launched to reach Saturn. The main goal of the mission was to study the planet, its moon, Titan, and determine structure and behavior of the planet's rings. As secondary objective it detected cosmic and interplanetary dust between 0.7 and 1.2 AU, and in the Saturnian system. The Cosmic Dust Analyzer (CDA), used during the mission, was an upgrade of the DDS, able to measure also the composition and electric charge of a particle. A total of 50 particles were detected. The dust measurements collected by Helios, Galileo, Ulysses and Cassini have been used to validate the Interplanetary Meteoroid environment for EXploration model (IMEX), with overall good results. Fluxes and size distributions simulated for time intervals and spatial regions, not covered in the original calibration, agreed with the in-situ measurements to within a factor of 2-3 [38].

In 1999, the Cometary and Interstellar Dust Analyzer (CIDA), and a Dust Flux Monitor

Instrument (DFMI) has flown on the Stardust spacecraft [62]. The main mission goal was to collect samples of dust and volatiles from the coma of the comet P/Wild 2, together with interstellar particles, and returned them to Earth. CIDA was a ionisation impact detector mounted on the side of satellite, while DFMI consist of a dust sensor unit based on PVDF and two acoustic sensors all mounted on the satellite front shield. Both instruments were used to directly analyse the composition, mass and flux of the comet ejecta. ESA's Rosetta mission [22] was the first to orbit around a comet and deliver a lander to its surface. The prime goal was to help understand the origin and evolution of Solar System by studying the comets composition. One of the instruments mounted was GIADA (Grain Impact Analyzer and Dust Accumulator), a combination of optical and piezoelectric impact sensors. It analyse number, mass, momentum and velocity distribution of dust grains in the near-comet environment.

Another study of the interplanetary particle respect to Sun distance has been operated by New Horizons satellite [20], during its journey to Pluto. The detection has been performed by an impact sensor based on 14 PVDF films, the Student Dust Counter (SDC). In 2018, ESA's mission BepiColombo [50] planned to study Mercury's environment. This was also a good opportunity to characterise the dust particle evolution in the inner orbits of Solar System. The Mercury dust monitor (MDM) was composed of piezoelectric ceramic sensors attached to the side panel of the magnetospheric orbiter.

Next year, ESA's Hera mission [17] will leave to the Didymos system, to survey the aftermath of a collision by NASA's DART spacecraft with the smaller of the two asteroids, Dimorphos [27]. Hera will carry two 6U CubeSats : Juventas and Milani. The former for radar soundings; the latter to get images of the asteroids body, identifying variation in surface composition, DART's crater and ejecta included. In particular, Milani will carry also an italian-built dust detector, VISTA (Volatile In-Situ Thermogravimetre Analyser), devoted to detect dust particles smaller than 5-10 μm, volatiles such as water, characterise light organics and monitor the molecular contamination surrounding the CubeSat.

1.2.   Earth Region

Focusing on the near-Earth orbits, the characterisation of the space environment has started with the first American space program: the Explorer [55]. The program began in 1958 and at today count 99 successful missions, covering a variety of scientific investigations. One of the program objective in particular was to characterise the micrometeoroids population and the effect of their impact on the spacecraft. It is the case of the series S 55, launched between 1961 and 1964 in LEO orbit. The first one, Explorer 13 (S 55A) [52], was mistakenly placed in a lower orbit and after 2 days it re-enter without detection data. The Explorer 16 (S 55B) [53] lifetime instead was of 7.5 month, during which it successfully operated 5 experiment to obtain data on size, number, distribution, and momentum of dust particles. Among them the most productive were the Pressurized Cell Detector and the piezoelectric impact detector. The former used semi-cylindrical pressurised cells, with different thickness wall, to record micrometeoroid impacts, based on the pressure drop due to the helium escape. The latter, used piezoelectric sensors, mounted at the end of the satellite casing, providing 0.35 m^2 of detection area. A total of 15000 impacts were recorded. Explorer 23 (S 55C) was the last of the series, with a lifetime of one year. It carried a stainless steel pressurized-cell penetration detector and a sounding board's based impact detector. In 1972 the Explorer 46 (MTS) [54] was launched in LEO orbit with the objective to evaluate the effective of bumpers against meteoroids using a pressure penetration detector, and obtain data on particles velocity and flux by a couple of capacitor detectors. The experiment was a success even if due to energy problem the second experiment was shut down after one week, but not before recording more than 2000 impacts.

In 1965 the Pegasus Project was launched by NASA to study the frequency of micrometeoroid impacts by means of a constellation of three satellites [59]. The satellites were equipped with parallel plates capacitors that temporarily discharged when penetrated.

One of the first debris detection satellite was the Shin Jian 2 (SJ 2) [23], launched in 1981 by China in an high elliptical orbit. The primary objective was to study the dust and debris environment, and update the Chines space debris model. The impact detector consisted of a charge detector, collecting particle in 0.05 to 50 μm range, and a light detector, for 50 μm to 0.5 mm particle range.

In the early '80s the advent of the Space Shuttle increase the possibility of studying the effects of space radiations and debris impacts, thanks to its capacity of easily deliver and recover big payloads. These data were used to fill the uncertainties in components design due to the lack of environmental models [67]. In this optic, two important missions were operated by NASA and ESA respectively: LDEF [19] in 1984 and EURECA [16]

in 1992. The former operated for about 6 years collecting debris and small meteoroids, studying the effects of long space exposure on structure, materials and technologies. The latter operate for about 10 month on science life experiment, material, radiobiology and particles collection. Both spacecrafts surface were analysed after the retrieval to quantify the debris and meteoroid impacts. The final data were collected in database and used to model the space debris environment. Thanks to this missions it has been recognised that orbital debris components represents a serious and growing hazard to space operation, causing catastrophic collision and erosive damage.

The need to characterise sub-millimetre particles at unexplored altitude drove the development of the SPADUS instrument [71] aboard the ARGOS spacecraft [14], launched in 1999 on a Sun-synchronous orbit at 850 km altitude. The instrument consisted of two identical planar arrays of PVDF dust sensors in a time-of-flight arrangement, providing particles mass, velocity and trajectory measurement. The mission detected a total of 368 impacts over 739 days of SPADUS live-time, yielding an average flux of 0.50 impacts/day. Of these, 35 were D1-D2 events, 19 of which resulted in velocity and trajectory measurement [72]. Although there could be uncertainty in the mission results, SPADUS has established a first-quantitative picture of debris orbits encountered, and proved that PVDF arrays can provide useful results for the near-Earth particles characterisation.

From now on many instruments for debris detection were tested. They have flown at various orbit to validate and expand the available models. One example is DEBIE. It worked on the Proba 1 satellite [21] (2001-2021) providing data on the debris flux on a Sun-Synchronous elliptical LEO orbit. It was based on a combination of impact plasma and piezoelectric detector, with a sensitivity of $1 \times 10^{-14} g$. The results were dominated by noise events due to eclipse thermal effects and plasma detector's exitation, these were easily distinguishable and removed. The remaining results were consistent with previous missions and MASTER models [66]. A second version of the instrument was used in 2004 on the ISS. The resulting flux in this case were 10 times higher than the models, probably due to the detection of secondary particles from the station [47].

With the increase of space exploration and on-orbit satellites the debris number rapidly increase, so a continuous sampling was needed to understand the evolution of the LEO environment. The combination of microsatellite and impact sensor were a cost efficient way to maintain accurate data. They were able to access space frequently, at low cost, by using piggyback launch opportunities. Following this optics, the IDEA OSG 1 [18] was equipped with JAXA's Space Debris Monitor (SDM) [73]. It was a simple sensor to detect particle ranging from 100 μm to several millimeters, based on 3300 conductive stripes on a non-conductive thin film. The satellite was launched on 2017, but unfortunately never reach its orbit due to a launch failure.

In the mean time the NASA Orbital Debris Program Office (ODPO) has pushed for the design of the DRAGONS sensor [42], with the objective to fill the gap in knowledge for the debris population in sub-centimeter scale. It consisted on two layers of thin film covered in conductive stripes and a solid back stop plate, multiple acoustic sensors were attached to each layer. Particles crossing the layers were detected by the sensors and characterised by a time-of-flight measurement. In 2017 DRAGONS was placed on the ISS to detect particle from 50 μm to 1 mm.

The University of Texas has developed a 3U CubeSat, the ARMADILLO [15], with the aim of studying the sub-millimetre scale orbital debris. It mounted a Piezoelectric Dust Detector (PDD) [30], based on a combination of plasma detection and piezoelectric sensors. The CubeSat has been launched in 2019, but after the first beacon all other attempts to ping has failed. Only in 2022 the team were able to connect with Armadillo and made an health checkout. Overall the spacecraft resulted in good health even after some Single Event Upsets (SEU), and it still had the potential to accomplish its goals [45]. No data are currently available.

Currently ESA is projecting a small-sat mission to statistically measure the near-Earth sub-millimetre to centimetre space debris population using deployed large-area thin foil surfaces, in order to validate and improve space environment models. The idea consist of a couple of Kepton sails equipped with PZT sensors, and a set of optical cameras for hole analysis. [3]

The study of space debris provides a crucial information for planning space operations, but only few missions have investigated this problem. An improved debris detection system for CubeSats is needed to increase the understanding of the debris environment. Those systems need to provide an effective, low cost platform for in-situ data collection, and contribute to the safety of future missions.

A summary of the missions involved in the dust and debris detection science is presented in table A.1 in Appendix A.

2 | Requirements

2.1. Payload requirements

Performance and function of the debris detector are given in the following requirements :

F-001	Impactors with size larger than 1 μm shall be detected
F-002	Impactors with size lower than 1 mm shall be detected
F-003	at least 100 debris impacts shall be detected
F-004	Particles dimension, velocity and direction shall be characterised
F-005	detector shall be able to reconstruct the particle orbit when possible
F-006	detector shall be able to measure time of flight with a sensibility of at least 0.05 μs
F-007	The detector shall be directed towards the velocity direction
F-008	CubeSat shall provide an accuracy of 1 deg during operation

PHY-001 specify the maximum space that the payload can occupy inside the CubeSat.

PHY-001	the detector shall occupy maximum 4U of space

2.2.   Mission requirements

F-009	The operational life time shall be at least 1 year
F-010	In case of failure shall be ensure the re-entry in less than 25 years
OPE-001	The operational orbit shall be between 400 km and 1000 km altitude
OPE-002	The operational orbit shall maximise the impacts statistics

The operational requirements give the baseline for the orbit selection and evaluation process. To ensure a safe space condition, requirement F-011 should be considered a priority during the orbit selection.

2.3.   Cubesat requirements

PHY-002 and PHY-003 define the maximum weight and size of the CubeSat, as defined in the mission system design [2].

PHY-002	CubeSat mass shall be less than 24 kg
PHY-003	CubeSat shall be less or equal to a 12U
F-011	The Δv budget for de-orbiting shall not exceed 150 m/s

3 | Orbit Selection

The operational orbit selection process, for a CubeSat mission, is reported in this chapter, focusing on debris detection. The chapter will analyse the number of small particle that can be detected, based on flux and impact per year, and will present the natural decay study to be consistent with the 25 years rule of the space debris mitigation regulations [26].

3.1. Debris Analysis

The aim of the debris detection phase is to characterise the sub-millimetre particle environment, with diameter range between 1 μm to 1 cm. Spatial density, flux and impacts number evaluations are performed, using the ESA software tool MASTER 8 (version 8.0.3) [12], focusing on the *Spatial Density* and *Target Orbit* modes. The 2026 is assumed as operational year for the simulation.

3.1.1. Spatial Density

The first survey performed is the particles density analysis with respect to the orbit altitude. The aim is to understand the debris and meteoroids density distribution in the Low Earth Orbit (LEO) region. The input parameters assumed in the simulation are reported in Table 3.1.

	Selection
Mode	Spatial Density
Starting Date [dd-mm-yyyy]	01-01-2026
End Date [dd-mm-yyyy]	01-01-2027
Particle Diameter Range [m]	1e-6 to 1e-2
Altitude Range [km]	400 to 1500
Declination [deg]	-90° to 90°
Right Ascension [deg]	-180° to 180°
Debris Source	Condensed
Meteoroids Source	Grun

Table 3.1: Input parameters for the Spatial Density analysis with MASTER 8.

Figure 3.1 shows the results of the simulation. The debris curve displays an increasing trend with peak at 950 km, followed by a slow descents up to the upper altitude bound considered. The meteoroids curve follows a slow increasing trend, but in general it can be considered almost constant in the altitude spectre. The simulation also highlights that around the peak the man-made particle density exceeds the meteoroids one.
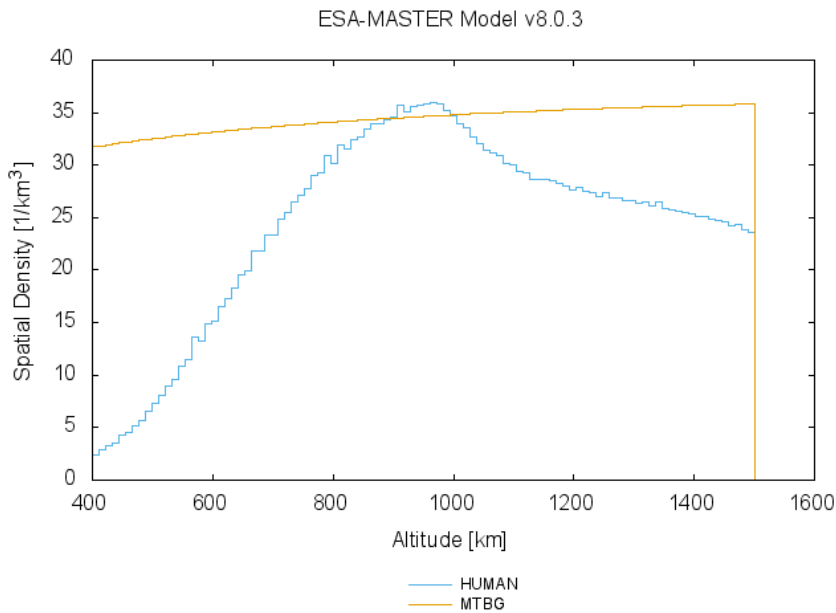

Figure 3.1: MASTER 8 : Spatial Density analysis

3.1.2. Flux Analysis

A more refines analysis is now performed focusing on the particle flux as function of orbit altitude and inclination. The simulation is computed with ESA MASTER 8, in *Target Orbit* mode. The study cover an altitude from 400 km to 1000 km, and inclination range, from 80° to 105°, around the Sun-Synchronous Orbit (SSO). The impact target considered is a flat surface oriented in the velocity direction. MASTER's input and the orbital parameter are summarized in Table 3.2 and Table 3.3 respectively.

	Min	Max	Type
Mode	-	-	Target Orbit
Selection	-	-	Earth-Bound
Argument of true latitude [deg]	0°	360°	-
Epoch [dd-mm-yyyy]	01-01-2026	01-01-2027	-
Resolution [year]	-	-	1
Particle Diametr Range [m]	1e-06	1e-02	-
Debris Source	-	-	Condensed
Meteoroids Source	-	-	Grun - Taylor distribution
Target Surface	-	-	Flat surface pointed in flight direction

Table 3.2: Input parameters to MASTER for flux analysis.

|	Value	Step
Altitude [km]	400 to 1000	50
Eccentricity [-]	0.0001	-
Inclination [deg]	80° to 105°	5°
RAAN [deg]	0°	-
Argument of perigee [deg]	0°	-

Table 3.3: Orbit parameter inputs to MASTER for flux analysis.

Figure 3.2 shows the results of the analyses. The particle flux is evaluated firstly as total flux (3.2a) and then separated as debris (3.2b), and meteoroids (3.2c). The red

line represent the SSO inclination. Total flux steadily increase with altitude, reaching the peak at 950 km. Along the inclination axis instead the flux show an almost constant trend, with slow variation, for orbit lower than 700 km ; while at higher orbit there is an increasing trend, reaching the peak at the SSO case. Looking at the two separated flux, the meteoroids show an almost constant trend with small variation in altitude; while the man-made particles reflects the same trend of the total flux case. This tendency suggest that the particle flux is dominated by man-made objects.
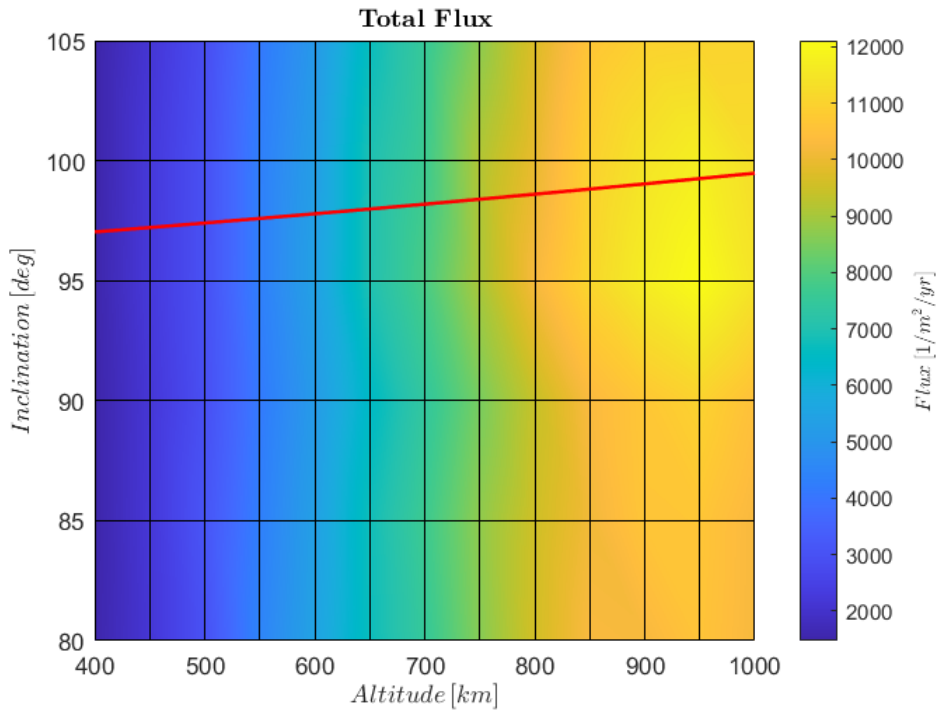
(a) Total Flux.
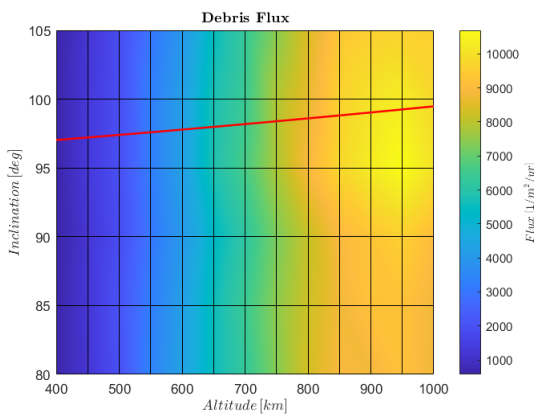
(b) Debris Flux.
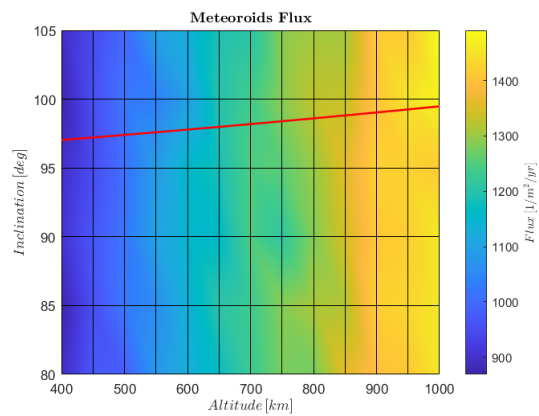
(c) Meteoroid Flux.

Figure 3.2: MASTER flux analysis, altitude vs inclination.

This preliminary analysis has pointed the SSO as the orbits with the higher flux. Additionally, these type of orbits are very busy, well served by launch opportunities, and of major interest for many missions. For these reasons SSO can represent a good target for a CubeSat mission. A more specific analysis on the fluxes in these region at different altitude is presented.

The first altitude considered is 500 km (figure 3.3a), the Sun synchronous inclination for a quasi-circular orbit is at 97.40° deg. At this orbit the cumulative debris flux is almost double respect the meteoroids one. Focusing on diameter of some μm, the two curve are comparable, while for dimension grater than 10 μm the MTBG curve flattens out and the man-made curve keep increase. Similar considerations can be done for the 550 km orbit (figure 3.3b). Sun synchronous inclination is 97.59° deg. The difference between debris and MTBG curve start to increase even at small diameter, and at end the cumulative debris flux result 3 times higher than the meteoroids. At this orbit an impact analysis can generate enough data to satisfy the mission requirement, to detect at least 100 debris impact.

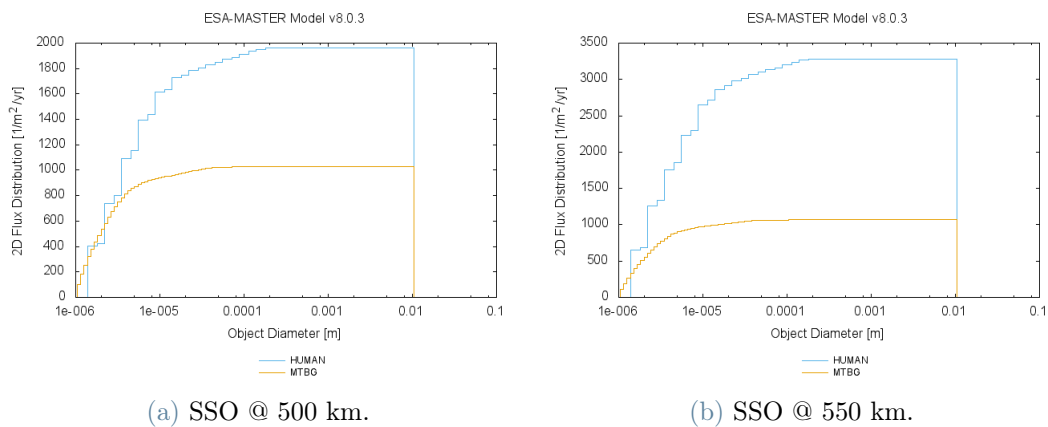(a) SSO @ 500 km. (b) SSO @ 550 km.

Figure 3.3: MASTER flux analysis: Cumulative flux vs particle diameter. Sun-Synchronous orbit at 500 km and 550 km altitude.

Increasing the altitude the situation is even better. At 600 km, and inclination of 97.79° deg, (figure 3.4a) the debris cumulative flux is 4 times the meteoroids one; while at 700 km, inclination 98.19° deg, (figure 3.4b) is almost 7 times.

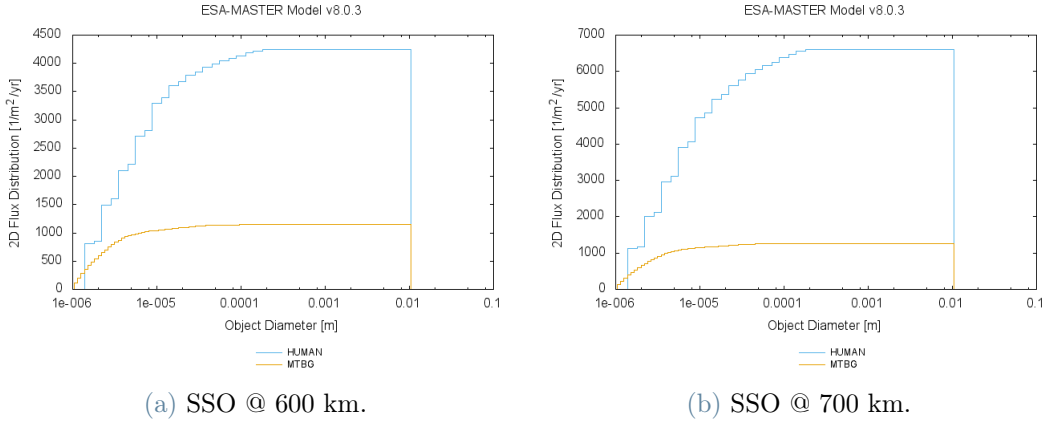(a) SSO @ 600 km.   (b) SSO @ 700 km.

Figure 3.4:   MASTER flux analysis: Cumulative flux vs particle diameter.   Sun-Synchronous orbit at 600 km and 700 km altitude.

At 800 km (figure 3.5a), the Sun synchronous inclination is 98.60° deg. The debris flux reach 9000 impacts per square meter per year, with the meteoroids fixed at 1000. In this region, "big" particles in the order of 100 μm, start to be more available. The characterisation of these particles would be of major interest, from the damage risk viewpoint. The climax is reached at 950 km with Sun synchronous inclination of 99.25° deg, shown in figure 3.5b. Here the debris cumulative flux is about 10 time as much as the meteoroids, with a final flux of almost 11000 debris per meter square per year. In this region the man-made flux considering only particle bigger than 100 μm is almost the same number of the total meteoroids cumulative flux.

(a) SSO @ 800 km.   (b) SSO @ 950 km.
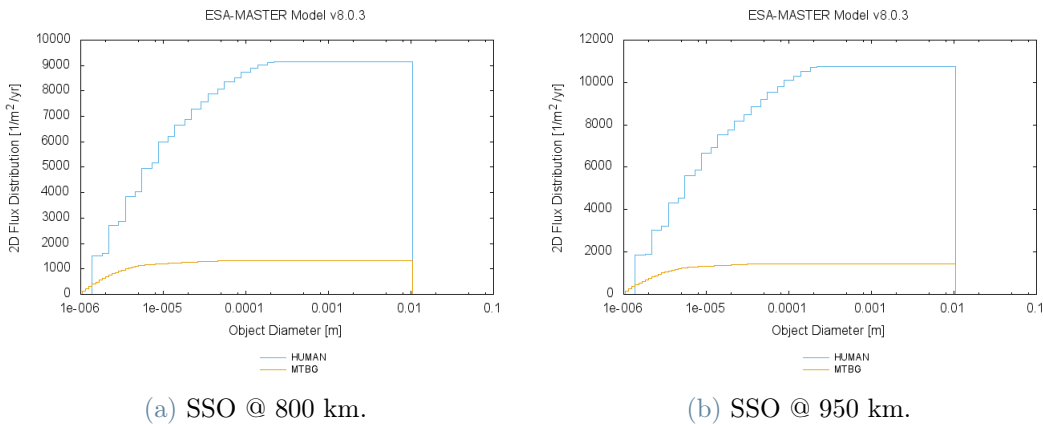
Figure 3.5:   MASTER flux analysis: Cumulative flux vs particle diameter.   Sun-Synchronous orbit at 800 km and 950 km altitude.

From the flux view point it is pointed that SSO at altitude equal or grater than 550 km

could be good targets for the mission, with the best option at 950 km, where is reached the peak of the flux and more bigger objects are present. In the next paragraph an impact analysis, based on the data registered in this section, is performed.

3.1.3. Impact Analysis

The number of impacts per year is computed as

$$N = flux \cdot A_c \tag{3.1}$$

where A_c is the impact area of the payload measured in m^2. For the analysis, the impact area has been considered as the front face of a 12U CubeSat equal to 0.04 m^2.

Figure 3.6 show the total number of impact per year, in an altitude versus inclination grid. As already seen for the flux analysis, most of the encounters are found in the higher orbits, reaching up to 500 impact/year. In very low orbit, under 500 km, the impact barely reach the 100 unit, too low for a good analysis. Central orbital region, between 500 km and 800 km, represent an intermediate situation.
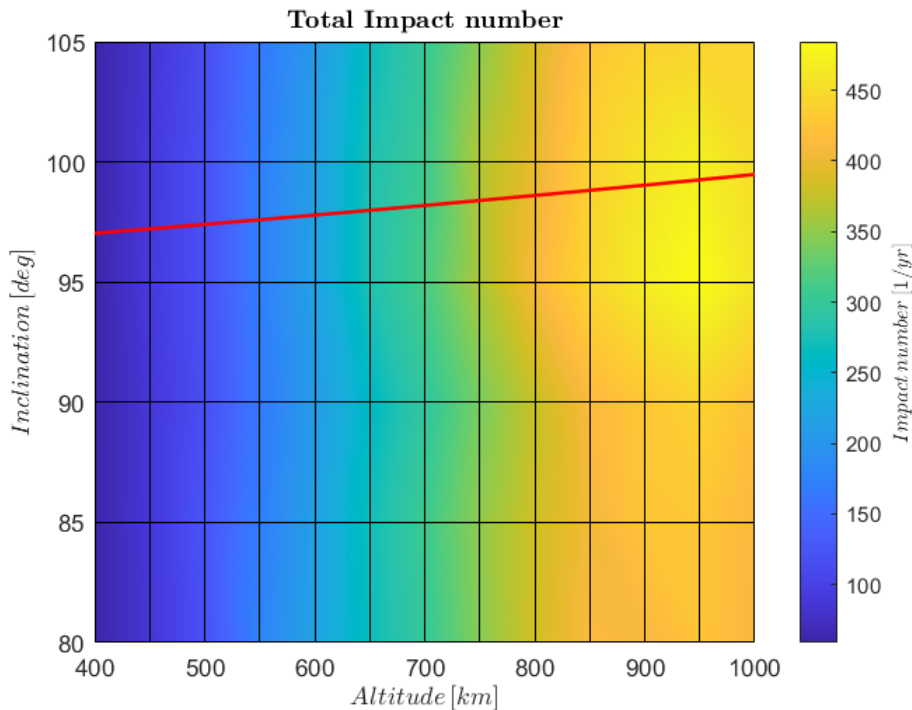

Figure 3.6: Impact analysis: altitude versus inclination.

From flux analysis in section 3.1.2 the SSO has been pointed as the best option, this

is particularly true for higher orbit and the impact analysis confirmed this statement.
Figure 3.7b shows the total impact difference between the SSO option and the second
best orbital plane. At lower orbits (less than 700 km), from the flux view point, 80 and
90 degrees of inclination would be a tiny better solution respect a SSO. However, the
difference in impacts number are very small (some units), so the Sun synchronous option
will be preferable. At higher orbit, instead, the SSO is confirmed to be the best case, also
from the impacts viewpoint. Figure 3.7a displays the impacts per year for the SSO case,
differentiating between MTBG and debris. As already stated, below 500 km the mission
requirements are not satisfied, while over 550 km the requirement of 100 debris impact is
reached.

(a) Sun-Synchronous orbit.   (b) Impact difference (SSO - best inclination).
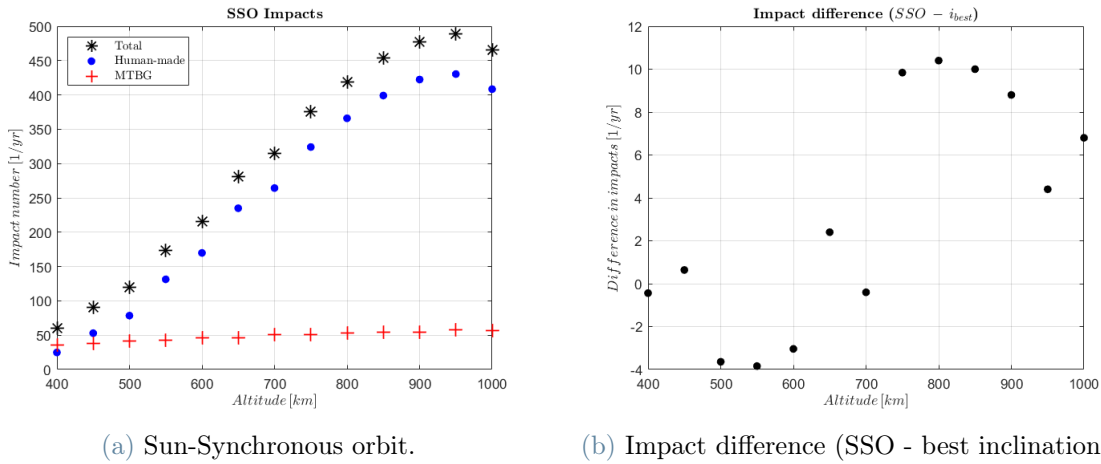
Figure 3.7: Sun Synchronous orbit impacts.

Final considerations are performed on different size of particle that can be encountered
on a SSO. Results are shown in figure 3.8. Most of the encounters are represented by
small particles, ranged from 1 to 10 μm, with impacts in the order of 10^2 per year. Below
700 km, the presence of bigger particle ($> 100~\mu m$) is very low, few units per year; while
at higher orbits their number is one order of magnitude higher. The resulted impacts per
year for a SSO are collected in table 3.4.

(a) Total Flux.

(b) Total Impact.

Figure 3.8: Total Flux and Impact vs altitude for different particle size.

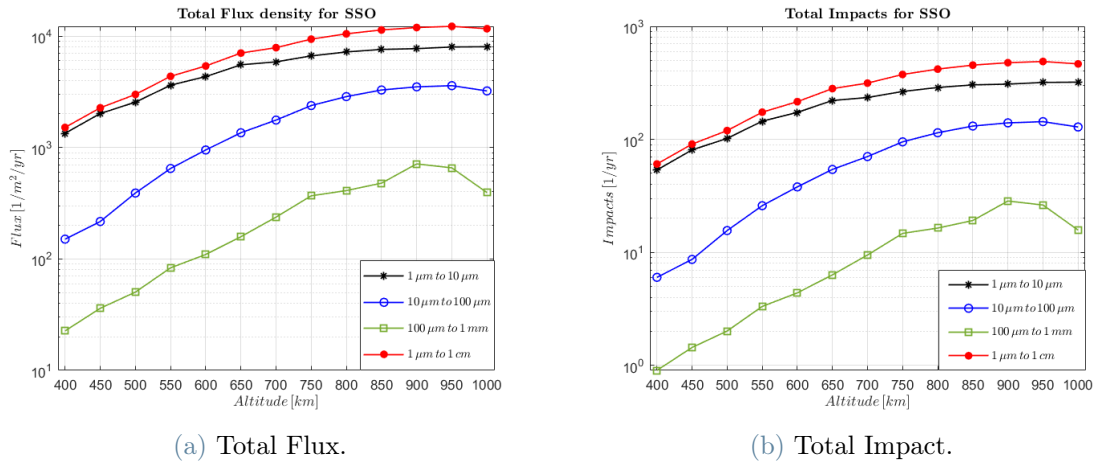|	$1\mu m - 10\mu m$			$10\mu m - 100\mu m$			$100\mu m - 1mm$			**TOTAL**
	MTBG	**Debris**	**Total**	**MTBG**	**Debris**	**Total**	**MTBG**	**Debris**	**Total**	**Total**
400 km	33	21	54	3	3	6	0.05	0.8	0.9	**61**
450 km	35	46	81	3	5	8	0.05	1.4	1.4	**91**
500 km	38	64	102	4	12	16	0.05	2	2	**120**
550 km	39	106	145	4	22	26	0.06	3.3	3.3	**174**
600 km	42	131.5	173.5	4	34	38	0.06	4.3	4.3	**216**
950 km	53	266	319	5	138	143	0.08	26	26	**489**

Table 3.4: Number of impacts per year.

As already expressed in the flux analysis, the perfect orbit for the mission, from a science point of view, would be an orbit between 850-1000 km altitude. In this orbital range in fact more particles are present, which means more scientific data, and also a great number of bigger particle that could be interesting from the satellite's risk view point. However the mission needs to be compliant with the debris mitigation regulations, so in the next section the CubeSat's natural decay will be analysed.

3.2. Natural Decay

In this section a simulation on the natural decay of the CubeSat has been performed to choose a working orbit compatible with the 25 year rule of the space debris mitigation. The CubeSat needs to be able to re-enter from the nominal orbit in less than 25 year, even in case of failure.

3.2.1. Perturbation model

To perform the analysis a MATLAB orbit propagation model has been developed. It considers a perturbed two body problem, under the effect of atmospheric drag and Earth gravitational perturbation (J2), as expressed in Eq.3.2

$$\ddot{\mathbf{r}} = -\frac{\mu}{r^3}\mathbf{r} + \mathbf{a}_{drag} + \mathbf{a}_{J2} \tag{3.2}$$

where $\mathbf{r}$ is the CubeSat position vector in km, μ is the Earth gravity constant (expressed in km^3/s^2), and $\mathbf{a}_{drag}$, $\mathbf{a}_{J2}$ are the perturbations due to drag and J2. The drag perturbation is computed in Eq.3.3

$$\mathbf{a}_{drag} = -\frac{1}{2}A_m C_D \rho v_{rel}^2 \frac{\mathbf{v}_{rel}}{v_{rel}} \tag{3.3}$$

where $\mathbf{a}_{drag}$ is the acceleration acting on the spacecraft due to drag, A_m is the cross area to mass ratio, C_D the drag coefficient, ρ the atmospheric density and v_{rel} the relative velocity between satellite and atmosphere.

During the analysis the perturbation due to the Earth oblateness has been also considered. The Earth is not a perfect sphere, but more like an oblate spheroid, flattened at the pole. This can be mathematically approximated assuming a zonal harmonic potential (distance r and latitude ϕ only dependent), and expanding it by an infinite series [9]. The resulting perturbation is expressed in Eq.3.4 :

$$\Phi(r,\phi) = \frac{\mu}{r}\sum_{k=2}^{\infty} J_k (\frac{R}{r})^k P_k(\cos\phi) \tag{3.4}$$

where J_k are the *zonal harmonics* of the planet derived from empirical observations, R is the equatorial radius, and P_k are the *Legendre polynomials*. The set of zonal harmonics is dominated by the J2 element, the largest one by far. For this resone in this thesis only the J2 effect has been taken into account, as J2 = 0.0010826359. The perturbing acceleration

resulting from this effect is expressed in Eq.3.5 :

$$\mathbf{a}_{J2} = \frac{3J_2\mu R^2}{2r^4}[\frac{x}{r}(5\frac{z^2}{r^2} - 1)\mathbf{i} + \frac{y}{r}(5\frac{z^2}{r^2} - 1)\mathbf{j} + \frac{z}{r}(5\frac{z^2}{r^2} - 3)\mathbf{k}] \tag{3.5}$$

The model has been propagated using the ODE113 function. A terminate condition at 100 km altitude is assumed. The ODE113 propagation will terminate if the orbit altitude reach this condition.

3.2.2. Atmospheric Model

The density at different altitude has been computed using an exponential model (Eq.3.6).

$$\rho(h, t) = \rho_0 e^{(\frac{h-h_0}{H})} \tag{3.6}$$

where the reference data are derived from different atmospheric models, based on the simulation to be done. The most generic one is the "U.S. Standard Atmosphere 1976" (USSA76) [63]. It is a static model that define the density change over a wide altitudes range. It is based on the assumption of an absolute temperature linear distribution in the atmosphere, without considering changes due to solar cycles and other factors. The second model considered is the Jacchia-77 model [35]. It includes geomagnetic and solar effects, and introduce the molecular composition correction. The model has been coded in Matlab by David L. Huestis (SRI International)[33], it estimates the atmospheric profile versus the altitude as function of the exospheric temperature, T_{EXO}. T_{EXO} can be derived empirically (Eq. 3.7) from the radio flux (F) at 10.7 cm, as index of the solar activity, with $\bar{F}$ being a smoothed F based on a Gaussian mean [29].

$$T_{EXO} = 5.48\bar{F}^{\frac{4}{5}} + 101.8F^{\frac{2}{5}} \tag{3.7}$$

Figure 3.9 shows the solar flux, F, and its Gaussian mean. The plot present also 3 possible flux prediction based on statistical estimate, and approximating the mean curve trend as a sinusoidal.
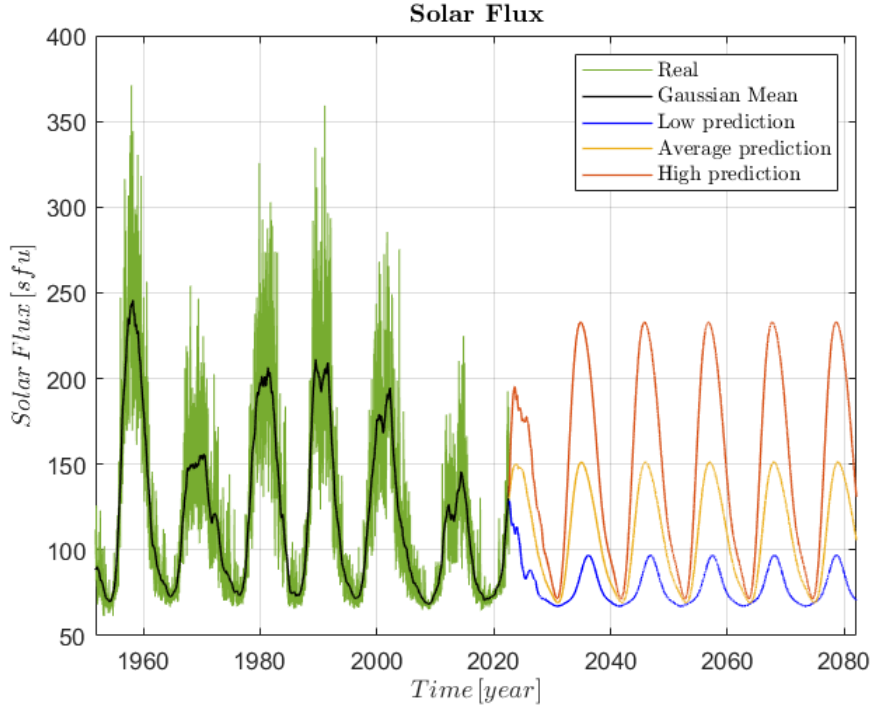
Figure 3.9: Daily 10.7 cm Solar flux from 1952, and prediction up to 2082 [61][69][43].

Based on this plot, the T_{EXO} used to calculate the atmospheric data, are derived with Eq.3.7, and listed in table 3.5 as minimum, maximum and mean value for each flux. The simulation is performed following the flux prediction trend. When the curve is in its bottom part, will be used the data from the minimum T_{EXO}; in the central zone the ones from the mean temperature; in the upper part the ones from the maximum Temperature. The flux model for the simulation is taken starting from the 2026.

	Low	Average	High
Min [K]	710	720	730
Max [K]	850	1060	1330
Mean [K]	760	890	1040

Table 3.5: Exospheric temperature input for the Jacchia-77 model.

The third model considered for the analysis make use of the CIRA-72. It use the USSA76 for the data at 0 km, CIRA-72 for 25-500 km and CIRA-72 with $T_{EXO} = 1000\,K$ for 500-1000 km [74]. Finally has been used the NRLMSISE-00 model to compare the results. It is one of the most complete model of the atmosphere. The simulation, for this model,

has been performed using the CNES's software STELA [4], following the daily variation of the solar flux prediction.

3.2.3.   Results

The first simulation (figure 3.10) shows the natural decay of different starting orbit using the USSA76 atmospheric model. For the analysis a 15 kg CubeSat has been assumed, with a cross sectional area of 0.08 m^2. The mass has been assumed from the attitude dynamics analysis by Francesca Scala et al. [65], considering a 20% margin on the preliminary mass budget. The cross sectional area has been computed using the *Area Tool* of the STELA software [4], assuming a random tumbling, and approximating the 12U CubeSat as a 20x20x30 cm cube. The orbits analysed are Circular SSO. Orbits higher than 700 km would take more than 100 years to decay so they are discarded. Orbits lower than 550 km take less than 15 years to decay, being compatible with the regulation; while a 600 km orbit present a re-entry in about 27 years. This would be slightly over the limit of 25 years imposed by the regulation, but it will still be considered for further analysis because it is close to the limit.

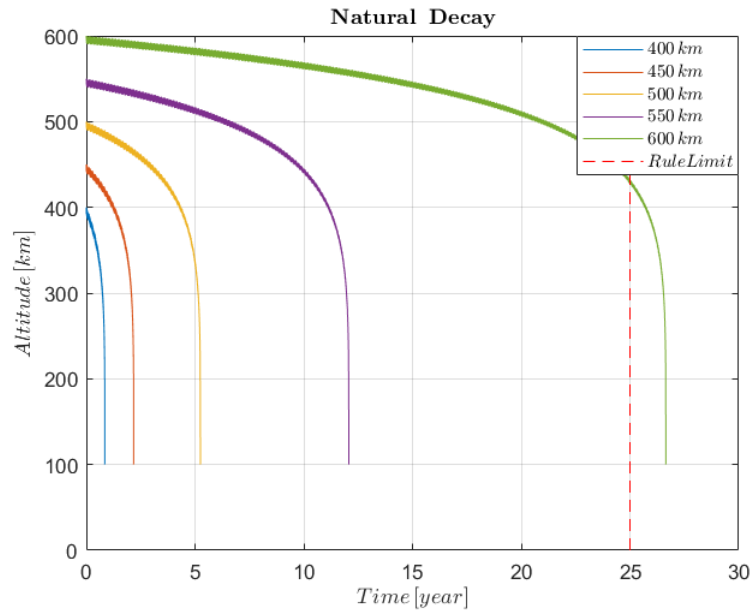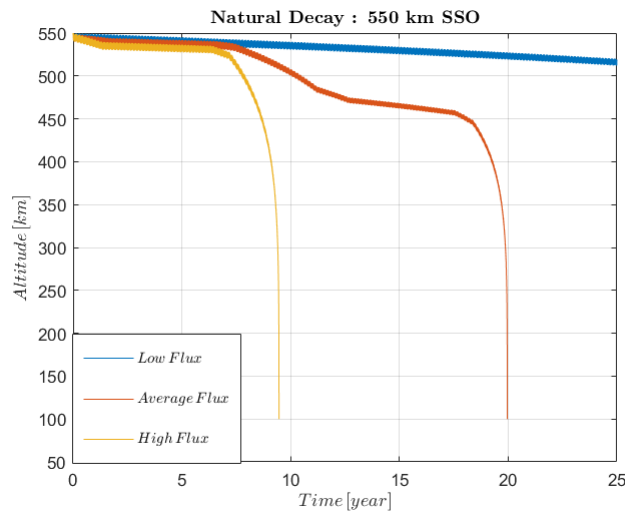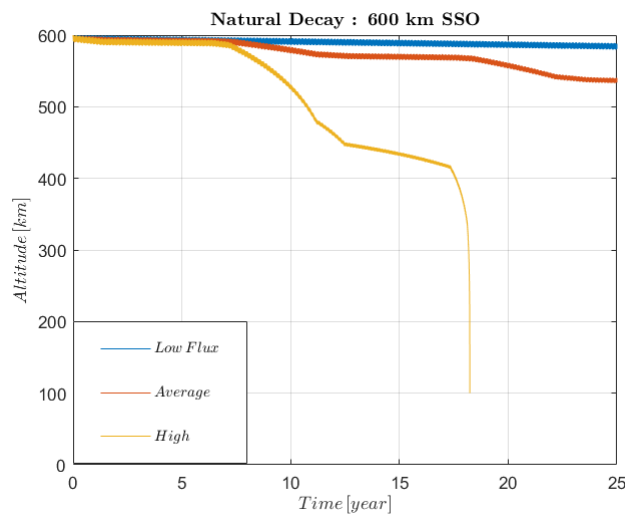Figure 3.10: Natural Decay - USSA76 model - m = 15 kg Area = 0.08 m^2.

At this point a comparison between different atmospheric models has been done. The focus will be on a 550 km and 600 km orbit, because between the case that may be able to re-enter, they are the ones that would return the higher number of impacts, based on the debris analysis in section 3.1. Figure 3.11 presents the decay based on the Jacchia-77

model reference data. Considering a low flux prediction, both orbital case would have a decay time too high. With an average flux prediction instead, the 550 km orbit is likely to decay about 20 years, while the 600 km orbit would require about the double. Finally, in the third scenario with an high flux prediction both orbit are likely to re-enter, the 550 km one with a decay time about 10 years, and the 600 km one in less than 20 years. However, it must be taken into account that the simulation is still based on statistical prediction of the flux and models approximations, so the result may differ from realty.

(a) SSO 550 km.

(b) SSO 600 km.

Figure 3.11: Natural Decay - Jacchia77 - m = 15 kg Area = 0.08 m^2.

Figure 3.12 presents a simulation where different models are compared. To the USSA76 and the Jacchia77, already expressed in the previous plots, are added other models. One

of the most accurate is the NRLMSISE-00, computed with STELA [4] following the daily solar flux variation. It results in a decay time of 13 years for the 550 km orbit (3.12a), and of 30 years for the 600 km one (3.12b). It is interesting to notice how the most general model of the USSA76 is the one that follow better the trend of a complex models like the NRLMSISE-00. For this reason in the last analysis, where the change due to the area to mass ratio will be studied, the USSA76 model will be used.
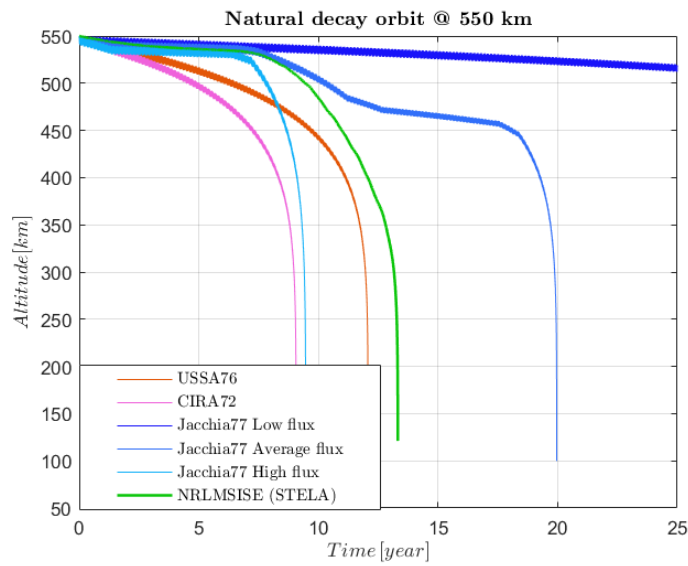
(a) SSO 550 km.
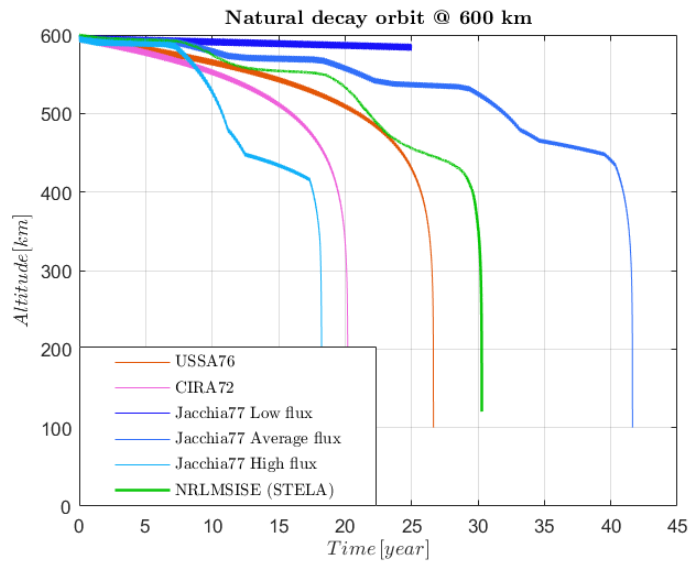
(b) SSO 600 km.

Figure 3.12: Natural Decay - m = 15 kg Area = 0.08 m^2.

The final simulation examines different mass and cross sectional area combinations. The CubeSat mass considered are 10 kg, 15 kg and 24 kg. They are assumed respectively from the preliminary mass budget [5], the attitude analysis [65] and the biggest acceptable mass from the requirement. For the cross section area to the already used 0.08 m^2, 0.09 m^2, and 0.1 m^2 will be added. Both area are calculated assuming a random tumbling with STELA [4], taking in consideration the presence of the solar panels wings. In the 550 km case (figure 3.13) all combinations decay in less then 20 years. The unsafer case is represented by the 24 kg option where an error due to the model or the area approximation could increase the decay time up to overcome the limitation. Looking at the 600 km case (figure 3.14), instead the only combination that re-enter in a good time are expressed by the 10 kg and 15 kg masses, with the latter being acceptable only for cross area with the solar panel. Even in this case a model or approximation error could result in a non re-enter inside the time limits.
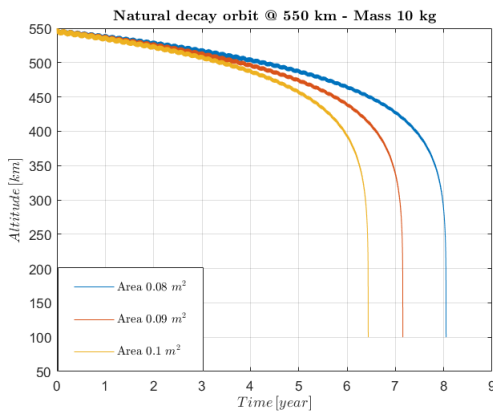
(a) Mass: 10 kg.
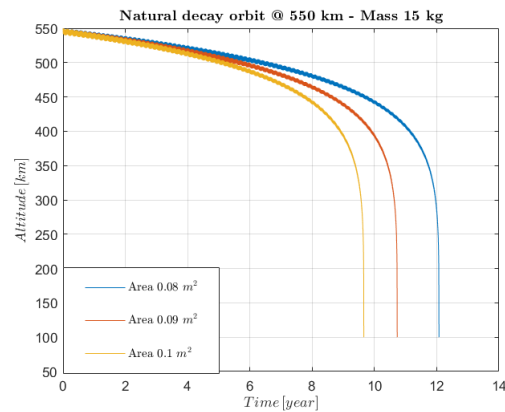
(b) Mass: 15 kg.
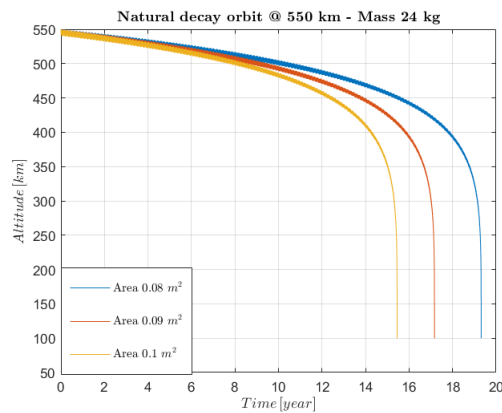
(c) Mass: 24 kg.

Figure 3.13: Natural Decay Area-to-mass ratio 550 km orbit.
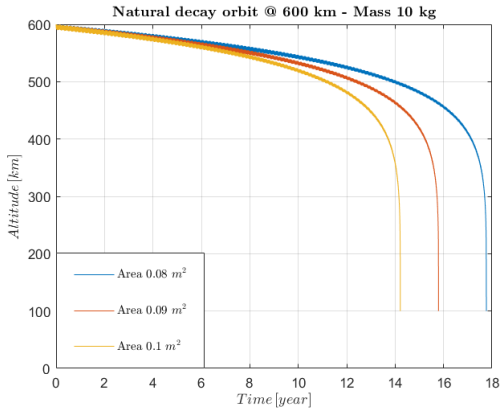
(a) Mass: 10 kg.
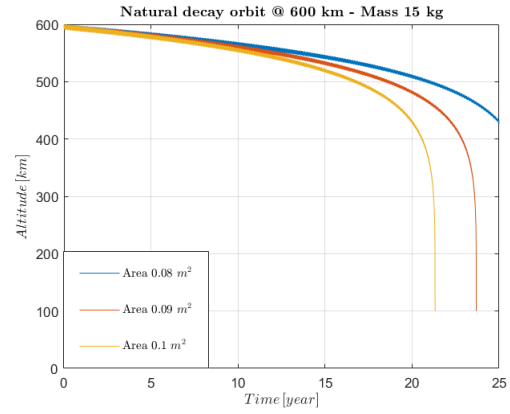
(b) Mass: 15 kg.
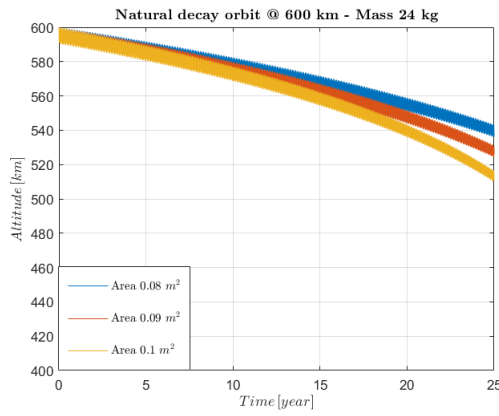
(c) Mass: 24 kg.

Figure 3.14: Natural Decay Area-to-mass ratio 600 km orbit.

Both orbits could be a good target for the mission, however based on the analysis performed the 550 km orbit is safer option, from the decay point of view.

3.3. Final Orbit Profile

The final orbit profile of the mission is based on the consideration of the debris analysis and the 25 years decay rule. A trade-off solution that can satisfy the mitigation guidelines and optimise the detection results is proposed. To maximise the debris impacts on the detector, an orbit between 900 km and 1000 km would be the best choice. However, to ensure a safe mission, compliant with the debris mitigation guidelines, an upper altitude boundary of 600 km shall be set. In this range the best option is to choose the maximum altitude possible, but as already seen in section 3.2 a 600 km orbit is at the boundaries of a 25 years re-entry, founding its decay time on the atmospheric models and cross-sectional area approximations. For this reason a more safer operational orbit is settle, reducing the amount of impact data collected in favor of a safer space environment.

The final orbital parameter are reported below:

- Semi-major axis: 550 km

- Inclination: Sun-synchronous [97-98] deg

- Eccentricity: Circular

The selected orbit is also compliant with the maximum ΔV de-orbit requirement of 150 m/s, as analysed in the Mission Analysis performed by M.P. Brenna [2].

4 | Payload Analysis

In this chapter, the preliminary analysis for the selection of the debris detection payload is presented. The aim is to provide an overview of possible payloads based on the literature, pointing advantage and disadvantage of each one, and provide a final choice for the mission profile.

4.1. Detection Method

Due to the increase of small orbital debris that can not be tracked by ground-based radars, a mitigation strategy based on in-situ detectors is required to characterise and model the orbital environment, minimising the failure risk for future missions. The primary distinction that can be done is between active and passive detectors. The letter is usually performed when pieces of large satellite are retrieved at their end-of-life, and a statistical population analysis is assessed by studying the damages on the structure. It is the case of EURECA [16] and LDEF missions [67]. This method however gives only average data, based on the spacecraft's orbit and lifetime. Furthermore, it is necessary to retrieve the satellite to apply this method. This would mean that the structure need to safely re-enter the atmosphere. This solution would complicate too much the mission profile, so an active detection is sought. Active in-situ detectors are widely used since the begin of the space era, as seen in chapter 1. They make use of different working principle and technology, like:

- Ionization Impact detectors
- Piezoelectric sensors
- Resistive wire grid
- Optical fence
- Light flash detectors
- Calorimetric Impact Energy detectors.

A brief overview of some methods is listed in table 4.1, characterising advantages, disadvantages.

Method	Work Logic	Advantages	Disadvantages
Ionization Impact	Particle properties are determined by the detection of the plasma cloud released by the impact with solid target.	• Well tested and reliable method • High mass range sensitivity • Unsensitive to thermal variations	• Sensible to plasma and environmental noise • Low accuracy on impact velocity and trajectory
PVDF	Piezoelectric thin film subjected to depolarization when impacted by HVI particle. It has an electric field frozen in an electret which is locally destroyed by impact. Two electrodes on either side detect this loss as a small charge fluctuation.	• Physically and chemically stable • Thermally and electrically stable • radiation resistant • relatively low cost • light and simple system • reliable	• require a second sensor for better accuracy

Method	Work Logic	Advantages	Disadvantages
PZT	They are typically a small ceramic lead titanate/zirconate plate or cylinder, self-energising, that provides voltage output proportional to the compression of mechanical wave produce by impact.	• High sensitive with low resource requirements • No power needed • Relatively low cost	• Require array of sensor to triangolate impact position • sensible to acoustic and thermal noise
Optical Fence	It consists in photodiodes that detect the particle scattered light when it pass through a laser/light curtain.	• Not invasive detection • Good velocity and trajectory accuracy, if combined with secondary sensor	• secondary sensor required for mass and velocity info • Relatively high power demanded
Electric wire	Detect the impact location by monitoring the wire conductivity. The particle size can be related to the number of electric strips that are cut.	• Simple • Low cost	• Need to be powered • Particle size estimation dependent on wire separation • Problems of multiple detection on same line

Method	Work Logic	Advantages	Disadvantages
Calorimetric Impact Energy	The energy conversion from kinetic to thermal during impact leads to a temperature rise of an absorber element. This rise, proportional to the absorbed energy, is measured by temperature sensors.	• Low environment noise interferance • Good detection accuracy	• Currently only lab tested • Relatively high power demanded • Sensitivity dependent on absorber thickness • Relatively expensive
Light Flash	Detect and measure the light intensity of an impacting particle on a known target material.	-	• Complex system • Susceptible to light noise • Needs of highly sensitive sensors

Table 4.1: Overview of particles detection methods.

4.2. Sensors Overview

Based on the detection methods analysed, an overview of specific impact sensors is provided in this section. The selection comprise either one type of sensor or an hybrid solution that combine multiple detection methods.

4.2.1. Ionisation Impact with PZT

The ionisation impact sensor is based on an impact target and a plasma detector. When a particle hit the target surface, it generates a plasma cloud of charged ions that can be detected and analysed to determine the impact properties. Piezoelectric material instead are a self-energising sensors that provide a voltage output proportional to the compression of a mechanical wave produce by the impact, and it can be associated to the particle momentum. This combination of sensors has been widely used on Proba 1 satellite, and than tested for the CubeSat format by Armadillo.

DEBIE

DEBIE was the instrument used on PROBA-1 satellite and on the ISS. The instrument consists of a Data Processing Unit (DPU) and up to 4 Sensor Unit (SU). Each SU provide the electronics for three plasma detector channels, two piezoelectric transducers and two temperature sensors [39]. The sensor sketch is shown in figure 4.1.
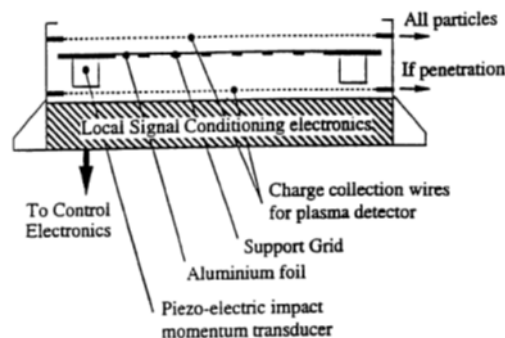
Figure 4.1: DEBIE sensor conficguration. Credit: Leese et al. [41].

The impact target is made of a 6 μm thick aluminium foil, glued on a supportive grid. Two PZT are attached to the corners of this grid measuring the impact momentum. In front and behind the foil two plasma stages registered the ions cloud. Finally in the topmost position there is the grounded grid which provides shielding against fluctuating plasma [66].

DEBIE specification are listed below [39] :

- Mass

  - SU: 560 g

  - DPU: 740 g

- Dimensions

  - SU: 157 x 135 x 47 mm

  - DPU: 156 x 136 x 42.5 mm

- Power (with 4 SU): < 4 W

- Operational Temperature: -30 °C to +55 °C

- Detection Area: 100 cm^2/SU

- Sensitivity (velocity dependent)

  - Plasma channel: 10^{-15} g

  - PZT channel: 10^{-14} g

ARMADILLO's PDD

The PDD used in the ARMADILLO mission is a detector specifically designed for Cube-Sat. The working concept is similar to the DEBIE sensor, but the impact target is directly represented by the PZT plate. The instrument structure is shown in figure 4.2. It consists of two Detector Units, a Main (MDU) and a Secondary (SDU), both connected to a central control unit (DCU). The MDU is structured with 9 piezo elements and two grids wire, with the top one acting as protective shield and ground. The second grid is charged and provide a signal based on the plasma produce by the impact. The SDU has a similar structure but use only one piezo plate.[40].
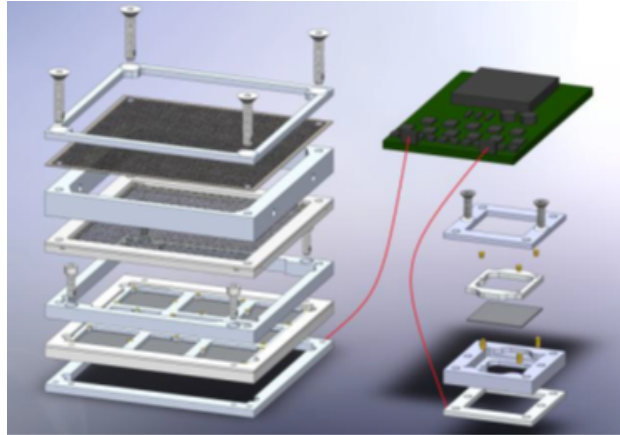
Figure 4.2: PDD structure MDU, SDU and DCU. Credit: Laufer et al. [40].

Payload characteristics are listed below [64][40]:

- Mass: about 400 g

- Dimensions: 80 x 80 x 40 mm

- Power: 3 W

- Piezo element: PZT-5 plate (21 x 21 x 0.55 mm)

- Data volume: 150 kbyte/day

- Sensibility

    - Particle size: 1 μm to 1 mm

    - Velocity: up to 10 km/s

    - Impact Energy: $< 1J$

4.2.2.   Trans-film with Electric grid and Piezo-elements

The concept of electric grid used to characterise the number of impacting particles and their dimensions, has been used in different missions like Horyu-II [28], IdeaOSG 1 [73] and also applied to the solar panel with the SOLID concept [1]. The impact surface is coated with long and thin resistive lines, when an impact occur several lines are cut. The hole size can be determined based on the number of braked lines, and under some hypothesis it can be related to the particle dimension. The biggest problem with this method is that once a line is cut it can not detect any other impact on that same line, limiting the analysis. The combination of electric wire with piezoelectric sensors has been used for the DRAGONS detector placed on the ISS [31]. A sketch is illustrated in figure

4.3. It consists of two thin films located 15 cm apart and a solid backstop plate at a short distance below the second film. Multiple acoustic impact sensors (PZT) are attached to the films and the solid plate. The film surface is also coated with long and 75-micron wide resistive lines. When a hypervelocity particle, sufficiently larger than the films and the wire, hit the first surface, it will cut one or more string, pass through the two film and hit the back plate. Impact location can be derived from the broken lines and a triangulation algorithm based on signal arrival time from the PZT. The combination of impact time and location provides the impact speed and direction. Experiments have shown that, for thin film penetration, the damage area is 5-10% larger than the particle, so the number of wire broken can be a good estimate for the particle size. Finally during the back plate impact, kinetic energy can be estimated by the PZT signal, and when the data are combined all the impact information can be obtained [31].
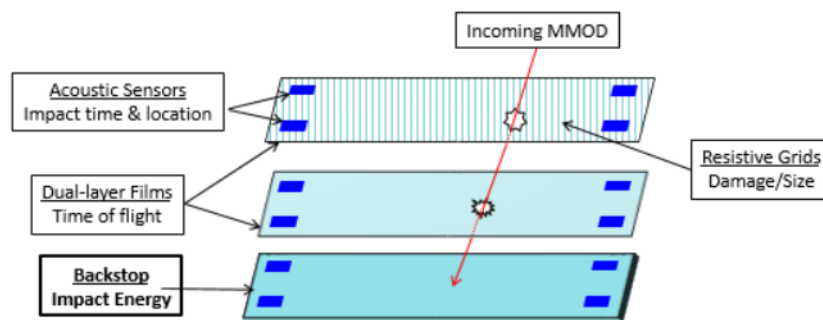
Figure 4.3: Three layer DRAGONS structure. Credit: Hamilton et al. [31].

Current instrument characteristics are summarised below [31] :

- Mass: 3 kg

- Power: 2 W

- Impact area: 1 m^2 (4 x 0.25 m^2)

- Data rate: 448 kb/day

- Sensibility: 50 to 500 μm

It is not specified if the characteristics are related to one 0.25 m^2 panel or to the final instrument composed of 4 panels.

4.2.3.   Optical fence with Impact detector

To obtain precise velocity data, measuring the Time-of-Flight (ToF) between two sensors, the first stage must preserve the integrity and dynamics properties of the particle. It is the case of the optical curtain based instrument, where the particle is detected by the light scattered produce crossing a light curtain. Two instrument are presented as possible reference: GIADA and AIDA.

GIADA

GIADA is the instrument flown aboard the Rosetta mission. Its structure is schematised in figure 4.4.

<table>
<tr><td>(a) GDS concept. Credit: Durin et al. [10].</td><td>(b) IS concept. Credit: Della Corte et al [8].</td></tr>
</table>
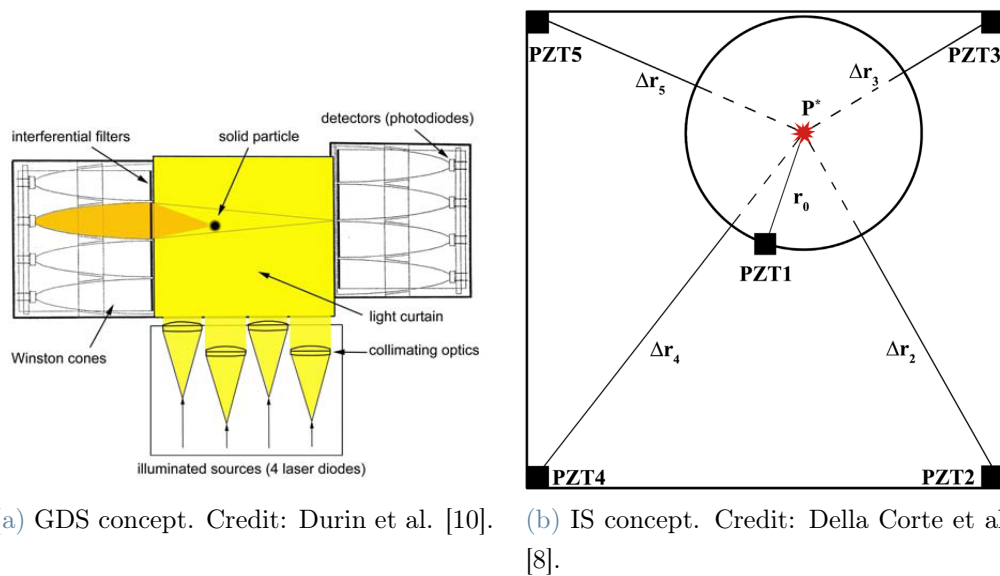
Figure 4.4: GIADA instrument concept.

It is composed by a Grain Detection System (GDS) and an Impact Sensor (IS). The GDS detect the individual particle entering GIADA, it consists of a 3 mm illuminated area of section 100 x 100 mm^2 generated by four laser diodes. The scattered light is detected by two series of four photodiodes placed at 90° respect to the laser propagation direction. Information on the optical equivalent size of the crossing particle are retrieved. After this first stage the particle impact on the IS, placed in cascade to the GDS. It is a sensing plate composed by 5 zirconates piezoelectric (PZT) glued under a 0.5 mm thick aluminium plate (100 x 100 mm^2). The 5 PZT detect the acoustic bending wave generated by the impact and giving information on the momentum of the particle. The ToF measured between GDS and IS provides the particle speed, and so its mass [8].

Payload characteristics are summarised as follows [7] :

- Mass: 5.90 kg

- Power: 20 W

- Detection Area: 0.01 m^2

- Sensibility

    - GDS (diameter range): 60 μm to 1 mm

    - GDS (speed): 1 to 300 m/s

    - IS (momentum): 6.5e-10 to 4e-4 kg*m/s

AIDA

The AIDA instrument [32] introduces some improvements on the second stage, reducing the environment noise by exploiting the calorimetric impact energy detector. The first stage is based on two laser light curtains, the particles passing through the light sheets cause flashes of scattered light, detected by a set of optical sensors. Measuring the ToF between the two sheets give information on speed and trajectory of the particle. The calorimetric impact stage is based on a gold absorber sheet and a thermopile sensor. The kinetic energy of the impacting particle is transformed into a rise of temperature, measured by the thermopile [32]. A theoretical represenatation of the two stage is presented in figure 4.5.

(a) First Stage - Oprical detection   (b) Second Stage - Calorimetric Impact Energy
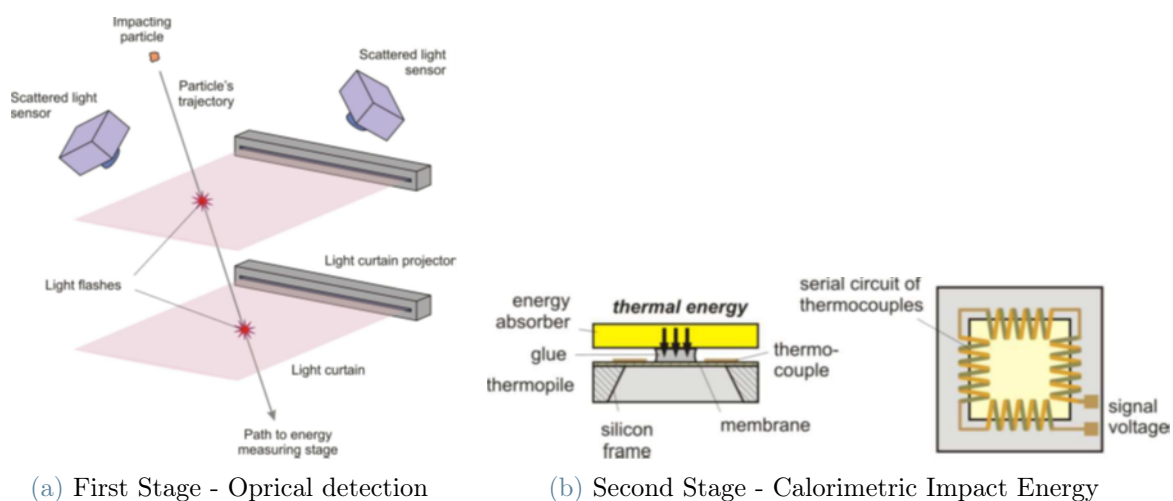
Figure 4.5: AIDA detectors concept. Credit: Herbst et al. [32].

The instrument has not been proved on orbit.

4.2.4. PVDF

The PVDF is a thin polymer film of permanently polarised material, with piezoelectric and thermoelectric effects, that undergo depolarisation when subjected to hypervelocity impacts (HVI), resulting in a fast charge pulse signal. This pulse can be used to localise the impact spot on the piezo-film [44]. PVDF has stable physical and chemical properties, is flexible, lightweight, and available in a wide variety of thickness. It is a relatively inexpensive material that can cover large area, and variety of shape [70]. The generic characteristics of the PVDF are listed below [70] :

- Relatively inexpensive, large area, flexible, thin films easily cut to variety of shapes/size;

- Areas up to 600 cm^2;

- Thickness from 1.5 to 800 μm;

- Density between 1.78 and 1.82 g/cm^3

- highly radiation resistant (immune up to 10^7 rad);

- fast response;

- chemically and physically stable.

This sensor has been used in different missions. For our purpose will be considered the possibility of using such sensor in a double stage arrangement like the SPADUS instrument [71].

1D PVDF: SPADUS

The instrument use 2 layers of PVDF sensors, in a time of flight configuration. Each layer is composed by 16 PVDF sensors, with thickness of 6 μm. The two layers are spaced about 20 cm. When a particle impact both layers, a ToF is measured and the particle speed can be calculated. From the speed all the particle characteristics are derived. If only the first layer is impacted the particle characteristics are estimated, assuming an impact velocity of 13 km/s. In this case the particle orbit can not be derived.
SPADUS characteristics are listed below [71] :

- Mass: 23 kg

- Power: 6.3 W

- 16 PVDF sensor per layer - 36 cm^2 each

- 2 layers spaced of 20.25 cm

- Particle size range: 2 to 200 μm of diameter

The instrument has shown poor accuracy on the detected velocity (up to 40% of uncertainties) [72], probably due to the big dimensions of the single PVDF foils and the low accuracy on the impact location detection. However, the mission has been declared a success for this sensor concept. For future missions with same concept, it has been stated that lower thickness of PVDF together with the 2-dimensional concept are required to increase the accuracy. Also, the use of a larger number of smaller sensors with the increase of the total sensitive area would provide excellent results [72].

2D PVDF

The 1D concept can be improved by introducing another dimension, using a grid-like system of electrodes. Although this approach is still in the conceptual phase and has only been tested in laboratory, the test results are promising. Narrow strips of aluminium foil electrodes are placed on the positive and negative side of the PVDF film. The electrodes are kept separated between each other, leaving small distances. On the same face they are placed in the same direction, while between the two sides are perpendicular. The strips of aluminium that is penetrated will produce and export a sharp pulse with large amplitude, while the one not impacted will export low voltage. In this way the location of the impact can be determined based on the coordinate of the responding electrode. Based on how thin and close to each other the aluminium foils are, this method can also provide a first estimate of the impactor size in case multiple strips are perforated [44]. A prototype for the double layer concept has been built and tested by Zhen Liu et al. [44] , figure 4.6.
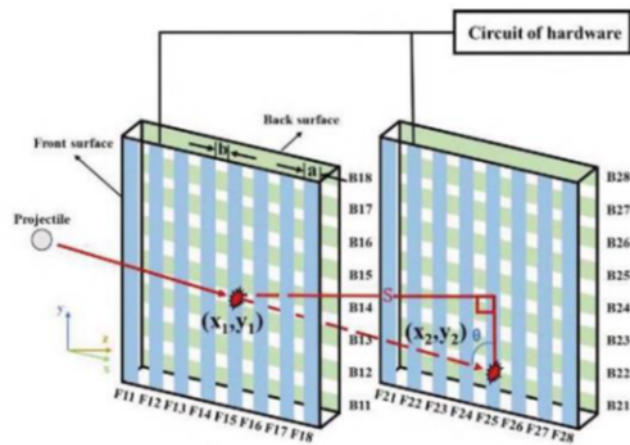
Figure 4.6: 2D PVDF concept in a double layer configuration. Credit: Zhen Liu et al. [44].

8 conducting strips (aluminium foil) of certain width and having gaps between them are placed on the front surface of each layer of PVDF, with an identical, orthogonal set on the back surface. Each aluminium foil is then connected to an external resistance, respectively, corresponding hardware circuit is designed. The signal produced by every strip will pass through the corresponding voltage comparator. Combining the information of first and second layer, the debris size, impact velocity, and angle can be calculated [44]. The sensor is installed with a separation of 80 mm between the two layers. The test showed promising result with relative error in range from 3-7% for the impact location, and about 3% error for the velocity estimation [44].

4.3. First trade-off

An overview of advantages and disadvantages for the impact sensors considered are provided in table 4.2.

Sensor Type	Reference instrument	Advantages	Disadvantages
Impact Ionization + PZT	DEBIE	• Trustable (well tested in orbit)	• sensible to environmental noise • Low accuracy on impact velocity and trajectory • small detection area • relatively heavy • need of impact plate target

Sensor Type	Reference instrument	Advantages	Disadvantages
	PDD	• Low Cost • CubeSat costumized • Sensor directly act as impact target	• Sensible to environmental noise • small detection area • PZT deterioration on impact
Film surface + Electric Wire + PZT	DRAGONS	• Accurate determination of impact location • Good velocity estimate using double stage configuration • Possibility to use PVDF as film layer	• Acoustic and thermal noise problems • Problems with multiple detection on catted lines • Particle size range dependent on wire characteristics and film thickness • Double stage CubeSat compatibility TBD

Sensor Type	Reference instrument	Advantages	Disadvantages
Optical + Impact detector	GIADA	• Good accuracy on velocity and mass estimation	• relatively heavy • Highly power demanded • CubeSat compatibility TBD
	AIDA	• Less environment noise interference • Good Accuracy	• Low TRL (only lab tested) • High cost • Relatively heavy • Highly power demanded
Double stage: 1D PVDF	SPADUS	• Relativelly simple system • Relativelly light system • good heritage	• Particle range dependent on PVDF thickness • Low velocity accuracy • Double stage CubeSat compatibility TBD

Sensor Type	Reference instrument	Advantages	Disadvantages
Double stage: 2D PVDF	-	- Accurate determination of impact location - Relativelly simple system - Relativelly light system - Good velocity and trajectory estimation	- Need of power for the grid system - Particle range (for velocity detection) dependent on PVDF thickness - Double stage CubeSat compatibility TBD
Single stage: 2D PVDF	-	- Accurate determination of impact location - Relativelly simple system - Relativelly light system - Compatible with CubeSat	- Need of power for the grid system - Low velocity accuracy - no trajectory info

Table 4.2: Sensors first trade off.

The use of a double stage detector would be the best solution in terms of accuracy of the data, thanks to the possibility to measure impact velocity using a time-of-flight method instead of relying on experimental test data. However, the two layers should be spaced enough to provide meaningful time measurements. Until now the separations used in past

missions are ranged between 100 and 200 mm, except for the 2D PVDF laboratory test that have used a separation of 80 mm. This ranges could represent a big restriction for small CubeSat, so the possibility of reducing the distance between the layers has been analysed. At first a MASTER analysis on the particle velocity has been performed. The result is shown in figure 4.7.
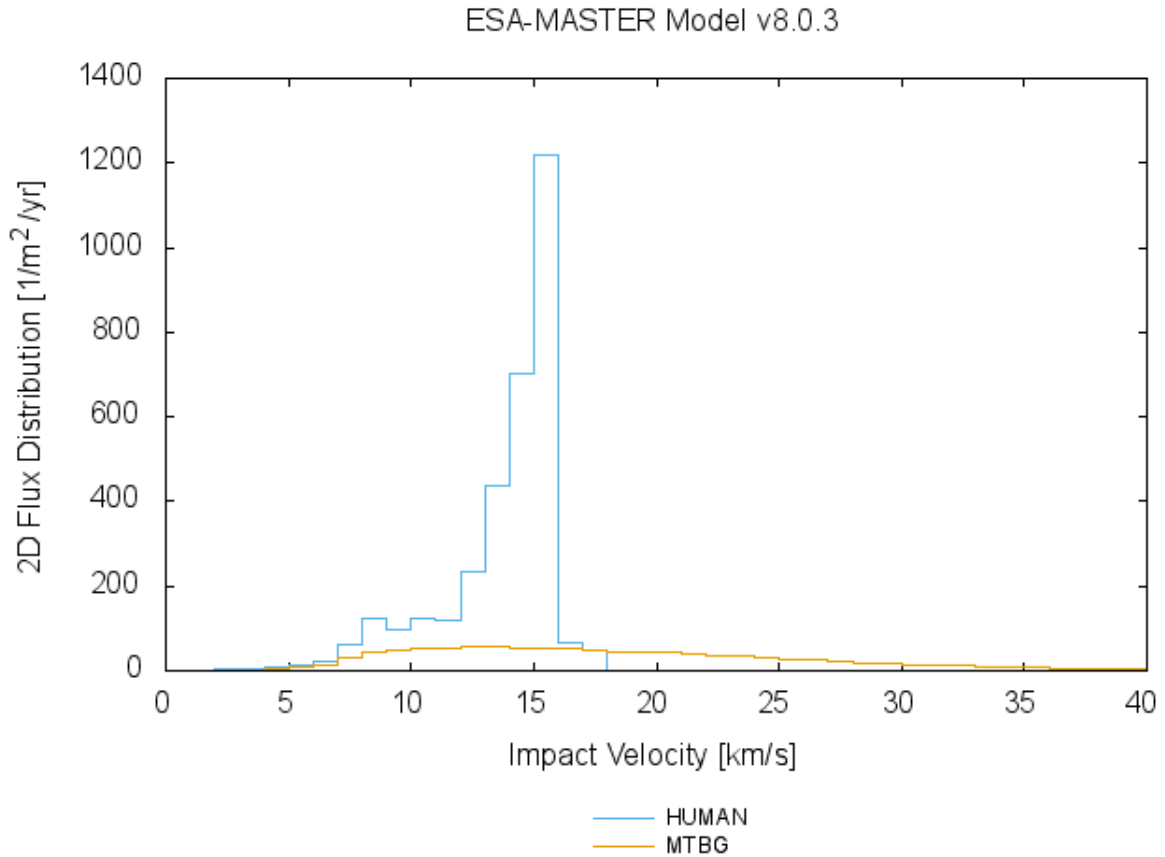
Figure 4.7: MASTER particle velocity analysis. Orbit: Circular Sun synchronous orbit at 550 km.

The orbit considered is the one selected for the mission in chapter 3, a circular Sun synchronous orbit at 550km altitude. The results show that the velocity range for man-made particles is between 5 and 20 km/s, with most of the objects at 15 km/s. A first approximation of the time-of-flight has been calculated as :

$$ToF = \frac{s}{v} \tag{4.1}$$

where s is the space between the layers in mm and v is the particle impact velocity in km/s, assuming that it does not change after the first layer. Impacts are assumed perpendicular,

so that the distance travelled by the particle is equal to the layer's separation, identifying the minimum measurable ToF. Results are listed in figure 4.8.
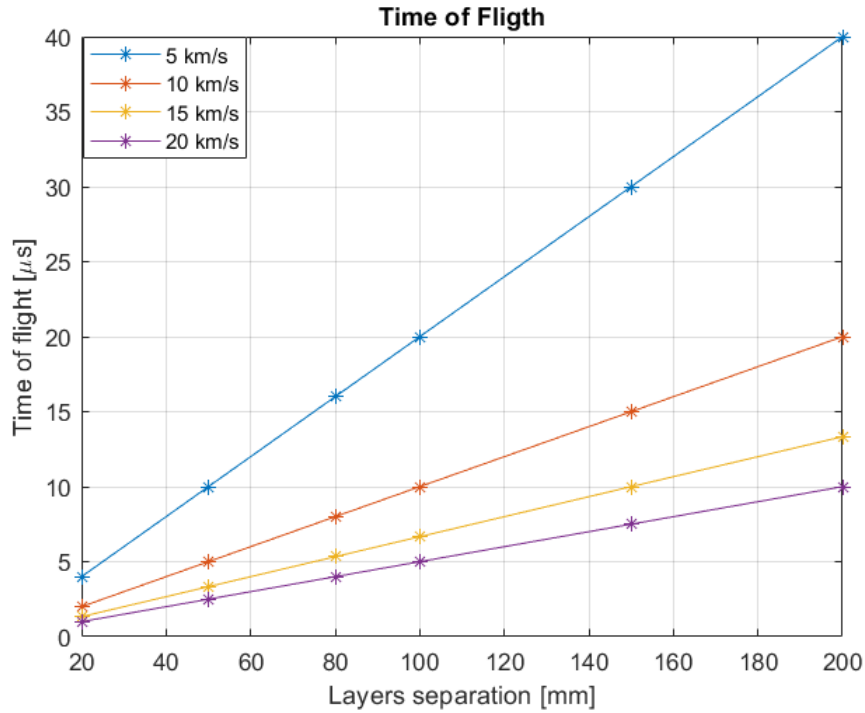
Figure 4.8: Time of Flight measurement.

It is identified that for small distances between the layers the resulting ToF is in the order of some units of microseconds. Based on the data set reported by SPADUS in 2005 [72], the clock used for the ToF measurement had a sensibility of 0.25 μs. This would make possible to measure such small time differences. Nevertheless, based on the technology improvement from 2005, a resolution of 0.01 μs could be currently reached. Anyway HVI tests should be done to evaluate the effective possibility to measure such small times with a good accuracy.

4.4.   Second trade-off and Baseline adaptation

The first trade-off analysis results in two possible solutions :

- Double stage configuration with 2D PVDF;

- Inization impact with PZT.

These concepts are further elaborated to identify the best fit for the study.

4.4.1.   Double stage 2D PVDF

The method presents similarities with DRAGONS and SPADUS instruments, so they can be taken as first baseline. For the mass we can scale the one of DRAGONS to the CubeSat detection area. For the power we can consider the power needed by SPADUS scaled to the detection area. The resulted characteristics are listed below :

- Detection Area: 0.04 m^2

- Mass: 0.5 kg

- Power: 4 W

4.4.2.   Ionization Impact with PZT

The baseline for this combination can be identified in DEBIE and PDD.

DEBIE

In this case 1 SU attached to the DPU could be used. The final characteristics would be :

- Total mass (SU + DPU): 1.310 kg

- Power: 1 W

- Detection Area: 0.01 m^2

the detection area in this configuration is 1/4 respect the CubeSat available area, so the #impact/year are 25% of impacts identified in section 3.1.3. Increasing the dimensions of the SU, adapting them to a 20 by 20 cm^2 surface, is possible to slightly increase the impacts detected. In this case, the detection area would be double, leading to the detection of 50% of the impact theorised in section 3.1.3. In this case the mass would increase of about 1 SU mass and the power needed would be double.

PDD

In this case it is possible to adapt the instrument increasing the number of PZT that are used as target, the solution analysed are with 25 PZT and 36 PZT. The final characteristics are summerised below :

- Dimension
  - 25 PZT: 133 x 133 x 40 mm
  - 36 PZT: 160 x 160 x 40 mm
- Total mass
  - 25 PZT: 1.1 kg
  - 36 PZT: 1.6 kg
- Power
  - 25 PZT: 8 W
  - 36 PZT: 12 W
- Detection area
  - 25 PZT: 0.011 m^2
  - 36 PZT: 0.016 m^2
- data rate
  - 25 PZT: 412.5 kb/day
  - 36 PZT: 600 kb/day

In both cases there is a low detection area and the #impact/year is between 25% and 40% of the MASTER analysis in chapter 3.1.3. The biggest problem with this set is the required power, that from a first analysis is 1.6 to 2.5 times higher than the budget allocated in previous document [2].

4.4.3. Comparison

The comparison between the solution is shown in table 4.3.

	Advantage	Disadvantage
DEBIE	• Good heritage • Low power	• Low detection area • Less science data
PDD (25 PZT) **PDD (36 PZT)**	• Designed for CubeSat • Good heritage	• power demanded • Low detection area, with less science data
Double stage: 2D PVDF	• Better performance • High detection area • Technology improuvement	• ToF to be tested • Needs a low mass backstop plate
Single stage: 2D PVDF	• High detection area • Technology improuvement	• No Impact direction information • Needs a low mass backstop plate

Table 4.3: Comparison between possible solutions.

Based on the analysis, the option proposed in this thesis is the Double stage configuration with the 2D PVDF sensor, because it is able to collect the required number of impacts and better characterise the impactor.

4.5.   Final payload preliminary design

The selected payload for the debris detection operation is a double stage detector with 2 foils of 2D PVDF sensors, in a time-of-flight arrangement, with an aerogel particle collector placed behind the second foil. The payload will be placed on the CubeSat's front face, and together with the electronics will occupy about 4U of space. A schematic view of the payload organisation is represented in figure 4.9.
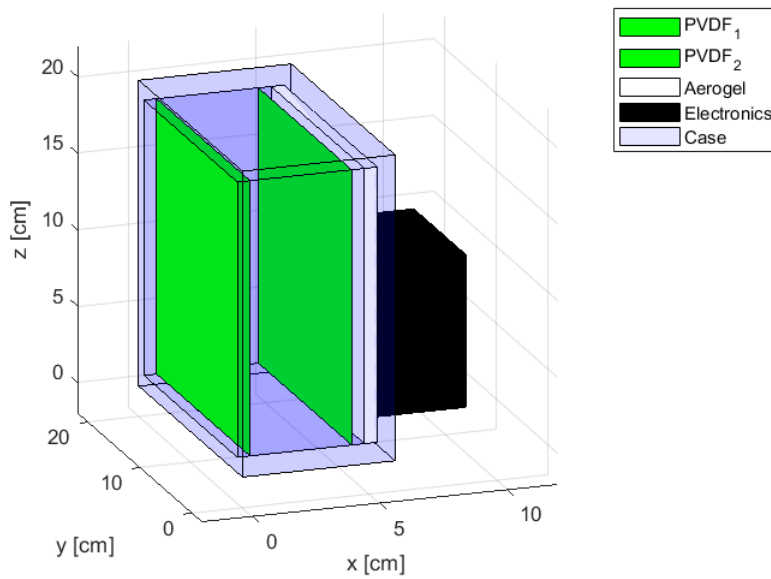
Figure 4.9: Payload schematic organisation.

4.5.1.   Size and Mass

The payload mass and size data are reported in the following table :

Parameter	Value
Sensor size	20 x 20 x 6 cm
Detection Area	0.032 m^2
Electronics size [5]	9.2 x 9.7 x 4 cm
Mass	1.6 kg (without the electronics)
Power	5 W

Table 4.4: Payload size and mass.

The single sensor is a 3 μm thickness PVDF foil, sandwiched with two layer of conductive

strips. The PVDF thickness has been chosen based on past experience, so that most of the particle can pass through without vaporise. Based on the analysis in section 4.3 on the time of flight measurement, the two PVDF stage will be placed with a distance of 4 cm between each other. This solution consent to have a relatively compact payload, keeping a good accuracy of the data.

Each PVDF is sandwiched between two layers of conductive strips, mounted orthogonal to each other. This allow a better determination of the impact location, increasing the sensor accuracy. The conductive strips are assumed to be made of 1 μm thickness aluminium foil. Width and pitch of the strips will be decide testing different configuration, and analysing their response. As first design two options can be considered :

- **Option 1:** 25 μm wide - 15 μm pitch

  The concept is similar to the DRAGONS instrument resistive lines. It estimates impact location and particle size based on witch and how many strips are cut. The biggest problem is that ones a strips is cut, it can no more detect particles on that same line, reducing the accuracy of the result.

  - Number of strips x layer: 4500 ;

  - Mass (4 layer): 0.2 g

- **Option 2:** 5 mm wide - 1 mm pitch

  In this case the concept is the one explained by Zhen Liu et al.[44], to improve the accuracy of a SPADUS like detector.

  - Number of strips x layer: 30 ;

  - Mass (4 layer): 0.3 g

The number of strips per layer and their mass are calculated on a detection area of 0.032 m^2. Both cases are valid options for the mission, but other combinations may also be tested. In this thesis the second option will be considered, because it can detect more particles impact on the same line, keeping the same accuracy for all the mission lifetime. The effect of impacts with bigger particles should be tested, however the probability of encounter such particle (> 1 mm) is very small.

Behind the second PVDF, a particles catcher will be placed to avoid secondary signal due to particle reflection. In a first approximation has been considered a 0.5 cm plate of silicon aerogel, with a mean density of 0.02 g/cm^3.

The sensor mass (PVDF, strips, aerogel) occupies only a small part of the total payload mass, most of it is characterised by the case structure. In a first approximation, based on similar instruments, it has been considered an aluminium box shape, with wall thickness

of 1 cm. In future works a specific structural design needs to be performed, focusing on reducing the structure total weight.

4.5.2. Power

The power needed by the payload is approximated analysing the power used by similar instruments. We can consider DRAGONS for the strips sensor and SPADUS for the PVDF target and the type of data recorded. Adapting their power to a detection area of 0.032 m^2, result that the power needed can be firstly guess at 5 W.

4.5.3. Impact detection

The payload should be able to detect particles in the range μm to mm. Based on the impact test on PVDF done by Tuzzolino et al. [70] for the SPADUS instrument, only particle bigger than 10 μm with velocity up to 10 km/s can survive the impact with the first stage and give a ToF measurement, determining impact velocity and direction. From the data returned from the ARGOS mission it seams that the velocity limit can be extended to 15 km/s. For smaller particle will be defined the flux, while characteristics like mass and size will be only estimated based on testing data and velocity assumption. The number of particle impacting the payload are reported in table 4.5, considering one year mission on a circular SSO at 550 km, and a detection area of 0.032 m^2.

	Debris	MTBG	Total
$1\mu m$ to $10\mu m$	86	31	117
$10\mu m$ to $100\mu m$	18	3	21
$100\mu m$ to $1mm$	2.65	0.05	2.7
$1mm$ to $1cm$	-	-	10^{-5}
TOTAL	**106**	**34**	**140**

Table 4.5: Impacts for a 550 km circular orbit. (based on MASTER data).

Based on the MASTER impacts results, almost 24 particles will return a ToF measurement, leading to precise velocity, mass and impact direction data. 117 smaller object will probably not survive the impact with the first stage so their size and mass will only be estimated based on velocity assumptions and testing data. The probability of a big particle to be detected can also be characterised. The Probability of No Penetration (PNP)

can be defined, starting from the impact flux as:

$$PNP = e^{-flux \cdot Area \cdot year} \tag{4.2}$$

It characterised the measure of survivability of a space object in function of size,geometry,structure, orbit and exposure time [28]. Its complement $(1 - PNP)$ could be used to characterise the impact probability of a specific particle dimension. For the size range from $100\mu m$ to $1mm$ the probability of impact is of the 93%, but only 11% for particle bigger than $200\ \mu m$. Going at the extreme the probability to impact a particle bigger than 1 mm is 0.009%, meaning that no sub-centimeter particle will be encounter. For this reason the payload is sized to detect particle smaller than 1 mm.

5 | Conclusions

This thesis discussed the preliminary design of the Debris Detection Phase for a CubeSat science mission in LEO orbit, focusing on the selection of the operational orbit and the payload. The operational orbit has been selected after a debris impact analysis, performed using MASTER 8. The objective was to guarantee a minimum of 100 debris impact by the detection payload. Sun synchronous orbits ranging from 550 km to 1000 km has been highlighted as potential targets. Consideration based on the debris mitigation regulations and on the natural decay time, have reduced the set to two possibility among which a Sun synchronous orbit at 550 km has been selected. The payload analysis has started with a literature review of past mission that have performed dust detection, identifying possible detection method and sensors combination that could perform the required debris characterisation. From the analysis performed, a doble stage 2D PVDF sensor in a time-of-flight configuration is selected. A first sizing of the payload is also proposed. The total detection area resulted is of 0.032 m^2, leading to a total of 140 predicted impact in the range 1 μm to 1 mm, 106 of which from debris.

CubeSat have a great potential for both science and commercial missions, reducing the cost and improving the compliance with space sustainability guidelines. The characterisation of the debris environment in LEO orbit, using CubeSats, could contribute to provide high fidelity models of debris distribution. They are a cost efficient way to perform the task, and represent a great opportunity for the sustainability of space environment, reducing operation cost and giving standard components to rely on.

5.1.   Future works

Future works should perform a complete payload design, based on the option selected in this thesis, focusing on the electronics design, the software for the computation of the data and the case structure. A complete design of the payload structure should be performed, minimising the total payload mass. The DRAGONS instrument could be used as baseline for the structure analysis, due to its low weight with respect to its big detection area. The payload detection area should not be decrease, to avoid a lower set of impacts data. The thickness of the PVDF should be kept as low as possible (under 6 μm) to increase the probability of a ToF measurement. A first breadboard model should be developed, and HVI tests should be performed to assets the functionality of the chosen payload, focusing on the time-of-flight measurement. Different configuration of strips materials and dimensions should be tested, starting with the option proposed in the thesis. A prototype should finally be developed.

Bibliography

[1] W. Bauer, O. Romberg, H. Krag, G. H. Visser, D. Digirolamo, M. F. Barschke, and S. Montenegro. Debris in-situ impact detection by utilization of cube-sat solar panels. *Small Satellite Systems and Services Symposium, Valletta (Malta)*, 2016.

[2] M. P. Brenna. Cubesat mission design for in-orbit environment characterisation. 2020. Politecnico di Milano, Supervisor: Camilla Colombo; Co-supervisors: Francesca Scala, Mirko Trisolini.

[3] A. S. Casado and M. Scheper. Dsbdm technology demo mission for deployable surface-based debris monitoring. final report.

[4] CNES. Semi-analytic tool for end of life analysis (stela). URL `https://www.connectbycnes.fr/en/stela`.

[5] C. Colombo, M. Trisolini, F. Scala, M. P. Brenna, J. L. Gonzalo, S. Antonetti, F. D. Tolle, R. Redaelli, F. Lisi, L. Marrocchi, M. Alberti, A. Francesconi, L. Olivieri, and M. Tipaldi. E.cube mission : The environmental cubesat. *8th European Conference on Space Debris (virtual), Darmstadt (Germany)*, 8, 2021.

[6] COMPASS web site. ecube - the environmental cubesat. URL `https://www.compass.polimi.it/research/ecube-mission/`. viewed : 15/08/2023.

[7] V. D. Corte, A. Rotundi, M. Accolla, M. Ferrari, S. Ivanovski, F. Lucarelli, E. Mazzotta-Epifani, F. J. M. Rietmeijer, and R. Sordini. Giada (grain impact analyser and dust accumulator): activity performed in support to the comet 67p/churyumov-gerasimenko encounter. *45th Lunar and Planetary Science Conference, Woodlands (Texas)*, 1777:2620, 2014.

[8] V. D. Corte, R. Sordini, M. Accolla, M. Ferrari, S. Ivanovski, A. Rotundi, F. J. Rietmeijer, M. Fulle, E. Mazzotta-Epifani, P. Palumbo, L. Colangeli, J. J. Lopez-Moreno, J. Rodriguez, R. Morales, and M. Cosi. Giada - grain impact analyzer and dust accumulator - onboard rosetta spacecraft: Extended calibrations. *Acta Astronautica*, 126:205–214, 9 2016. ISSN 00945765. doi: 10.1016/j.actaastro.2016.03.036.

[9] H. D. Curtis. *Orbital Mechanics for Engineering Students.* Elsevier ltd, 2014.

[10] C. Durin, J.-C. Mandeville, and J.-M. Perrin. In-situ detection of meteoroids and orbital debris. *European Space agency (Special Pubblication),* ESA SP-587:649–652, 2005.

[11] EoPortal, Orbital debris. URL `https://www.eoportal.org/other-space-activities/orbital-debris`.

[12] ESA. Space debris user portal - master. URL `https://sdup.esoc.esa.int/`.

[13] ESA, eoPortal. URL `https://www.eoportal.org/satellite-missions`.

[14] ESA eoPortal, ARGOS. URL `https://www.eoportal.org/satellite-missions/argos#esex-electric-propulsion-space-experiment`. viewed in : 15/08/2023.

[15] ESA eoPortal, ARMADILLO. URL `https://www.eoportal.org/satellite-missions/armadillo#pdd-piezo-dust-detector`. viewed in : 15/08/2023.

[16] ESA eoPortal, EURECA. URL `https://www.eoportal.org/satellite-missions/eureca#eop-quick-facts-section`. viewed in : 15/08/2023.

[17] ESA eoPortal, Hera mission. URL `https://www.eoportal.org/satellite-missions/hera#eop-quick-facts-section`. viewed in : 15/08/2023.

[18] ESA eoPortal, IDEA OSG 1. URL `https://www.eoportal.org/satellite-missions/idea-osg-1#eop-quick-facts-section`. viewed in : 15/08/2023.

[19] ESA eoPortal, LDEF. URL `https://www.eoportal.org/satellite-missions/ldef#eop-quick-facts-section`. viewed in : 15/08/2023.

[20] ESA eoPortal, New Horizons. URL `https://www.eoportal.org/satellite-missions/new-horizons`. viewed in : 15/08/2023.

[21] ESA eoPortal, Proba 1. URL `https://www.eoportal.org/satellite-missions/proba-1#eop-quick-facts-section`. viewed in : 15/08/2023.

[22] ESA eoPortal, Rosetta. URL `https://www.eoportal.org/satellite-missions/rosetta#giada-grain-impact-analyzer-and-dust-accumulator`. viewed in : 15/08/2023.

[23] ESA eoPortal, Shi Jian 2. URL `https://www.eoportal.org/satellite-missions/shi-jian#sj-2-shi-jian-2`. viewed in : 15/08/2023.

[24] ESA eoPortal, Ulysses. URL `https://www.eoportal.org/satellite-missions/ulysses#eop-quick-facts-section`. viewed in : 15/08/2023.

[25] ESA, Space debris by the numbers. URL `https://www.esa.int/Space_Safety/Space_Debris/Space_debris_by_the_numbers`. Last access : 24/08/2023.

[26] ESA Space Debris Office. Esa's annual space environment report, 2023. URL `https://www.sdo.esoc.esa.int/environment_report/Space_Environment_Report_latest.pdf`.

[27] ESA web page, Milani Cubesat (Hera mission). URL `https://www.esa.int/Space_Safety/Hera/CubeSat_will_sift_asteroid_secrets_from_reflected_sunshine`. viewed in : 15/08/2023.

[28] P. Faure, S. Matsumoto, Y. Akahoshi, M. Cho, T. Narumi, Y. Kitazawa, A. Sakurai, and T. Koura. Installation of an active debris sensor on a small satellite for in-situ space dust measurement. *AEROSPACE TECHNOLOGY JAPAN*, 2012. doi: 10.2322/tastj.10.tr_17.

[29] S. Frey, C. Colombo, and S. Lemmens. Extension of the king-hele orbit contraction method for accurate, semi-analytical propagation of non circular orbits. *Advances in Space Research*, 64:1–17, 2019. doi: 10.1016/j.asr.2019.03.016.

[30] K. B. Gamble and G. Lightsey. In-situ sub-millimeter space debris detection using cubesats. *2012 AAS Guidance and Control Conference*, 2012. URL `https://www.researchgate.net/publication/260798433`.

[31] J. Hamilton, J.-C. Liou, P. Anz-Meador, B. Corsaro, F. Giovane, M. Matney, and E. Christiansen. Development of the space debris sensor. *7th European Conference on Space Debris, Darmstadt (Germany)*, 7:1–11, 2017.

[32] C. Herbst, K. D. Bunte, T. Fichna, D. Hagedorn, G. Hemken, E. Keßler, and M. Kobusch. In-situ detector aida - advance, recent and future developments. *European Space Agency, (Special Publication) ESA SP*, 672 SP, 2009. ISSN 03796566.

[33] D. L. Huestis. Jacchia-77 matlab code. URL `https://www.mathworks.com/matlabcentral/fileexchange/54912-standard-jacchia-reference-atmosphere-1977`.

[34] D. H. Humes, J. M. Alvarez, R. L. O'Neal, and W. H. Kinard. The interplanetary and near-jupiter meteoroid environments. *Journal of Geophysical Research*, 79:3677–3684, 1974. doi: 10.1029/ja079i025p03677.

[35] L. G. Jacchia. Thermospheric temperature, density, and composition: New models. Technical report, Smithsonian Institution Astrophysical Observatory. Cambridge, Massachusetts, 1977. URL `https://ntrs.nasa.gov/api/citations/19770016704/downloads/19770016704.pdf`.

[36] D. J. Kessler and B. G. Cour-Palais. Collision frequency of artificial satellites: The creation of a debris belt. *Journal of Geophysical Research*, 83:2637–2646, 1978. doi: 10.1029/JA083iA06p02637.

[37] D. J. Kessler, N. L. Johnson, J. C. Liou, and M. Matney. The kessler syndrome: Implications to fuure space operations. *Advance in the Astronautical Sciences*, 137: 47–61, 2010.

[38] H. Krüger, P. Strub, N. Altobelli, V. J. Sterken, R. Srama, and E. Grün. Interstellar dust in the solar system: Model versus in situ spacecraft data. *Astronomy and Astrophysics*, 626, 6 2019. ISSN 14320746. doi: 10.1051/0004-6361/201834316.

[39] J. Kuitunen, G. Drolshagen, J. McDonnell, H. Svedhem, M. Leese, H. Mannermaa, M. Kaipiainen, and V. Sipinen. Debie-first standard in-situ debris monitoring instrument. *3th European Conference on Space Debris ESA SP-473, Darmstadt (Germany)*, 2001.

[40] R. Laufer, R. Srama, G. Herdrich, G. Lightsey, A. Wolf, R. Laufer, R. Srama, G. Herdrich, G. Lightsey, C. Wiedemann, T. W. Hyde, and H.-P. Röser. A modular, miniaturised, low-mass in-situ dust detector for piggyback payload opportunities on small spacecraft, landers and rovers. *63rd International Astronautical Congress, Naples (Italy)*, 2012. URL `https://www.researchgate.net/publication/289074171`.

[41] M. R. Leese, J. A. McDonnell, M. J. Burchell, S. F. Green, H. S. Jolly, P. R. Ratcliff, and H. A. Shaw. Debie - a low resource dust environment monitor. *European Space Agency, (Special Publication) ESA SP*, 1996. ISSN 03796566.

[42] J. C. Liou, R. Corsaro, F. Giovane, C. Anderson, A. Sadilek, M. Burchell, and J. Hamilton. Dragons – a micrometeoroid and orbital debris impact sensor. *Nano-Satellite Symposium (NSAT)*, pages 1–6, 2015. URL `https://ntrs.nasa.gov/archive/nasa/casi.ntrs.nasa.gov/20150019424.pdf`.

[43] LISIRD web page, NOAA Solar Radio Flux at 10.7 cm. URL `https://lasp.colorado.edu/lisird/data/noaa_radio_flux/`. viewed in : 11/09/2023.

[44] Z. Liu, W. X. Cao, W. B. Zhang, R. Q. Chi, B. J. Pang, and N. Yang. Double layered 2-d pvdf film based flexible sensor for detection of micro-space-debris: Impact

velocity, angle, and spot. *Proceedings of the 2020 15th Symposium on Piezoelectricity, Acoustic Waves and Device Applications, SPAWDA 2020*, pages 366–370, 4 2021. doi: 10.1109/SPAWDA51471.2021.9445541.

[45] D. Mcdonald, G. Lightsey, and S. Peet. Recovery of a lost satellite: The armadillo mission. *36th Annual Small Satellite Conference*, 2022.

[46] M. Mejia-Kaiser. Iadc space debris mitigation guidelines. *The Geostationary Ring*, 2021.

[47] A. Menicucci, G. Drolshagen, J. Kuitunen, Y. Butenko, and C. Mooney. In-flight and post-flight impact data analysis from debie2 (debris-in-orbit-evaluator) on board of iss. *6th European Conference on Space Debris, Darmstadt (Germany)*, 2:2–5, 2013.

[48] NASA. Space debris and human spacecraft. URL `https://www.nasa.gov/mission_pages/station/news/orbital_debris.html`.

[49] NASA, spacecraft catalogue. URL `https://nssdc.gsfc.nasa.gov/nmc/SpacecraftQuery.jsp`.

[50] NASA web page, BepiColombo. URL `https://nssdc.gsfc.nasa.gov/nmc/spacecraft/display.action?id=2018-080A`. viewed in : 15/08/2023.

[51] NASA web page, Cassini. URL `https://nssdc.gsfc.nasa.gov/nmc/spacecraft/display.action?id=1997-061A`. viewed in : 15/08/2023.

[52] NASA web page, Explorer 13 (S 55A). URL `https://nssdc.gsfc.nasa.gov/nmc/spacecraft/display.action?id=1961-022A`. viewed in : 15/08/2023.

[53] NASA web page, Explorer 16 (S 55B). URL `https://nssdc.gsfc.nasa.gov/nmc/spacecraft/display.action?id=1962-070A`. viewed in : 15/08/2023.

[54] NASA web page, Explorer 46 (MTS). URL `https://nssdc.gsfc.nasa.gov/nmc/spacecraft/display.action?id=1972-061A`. viewed in : 15/08/2023.

[55] NASA web page, Explorer program. URL `https://nssdc.gsfc.nasa.gov/multi/explorer.html`. viewed in : 15/08/2023.

[56] NASA web page, Galileo. URL `https://nssdc.gsfc.nasa.gov/nmc/spacecraft/display.action?id=1989-084B`. viewed in : 15/08/2023.

[57] NASA web page, Giotto. URL `https://nssdc.gsfc.nasa.gov/nmc/spacecraft/display.action?id=1985-056A`. viewed in : 15/08/2023.

[58] NASA web page, Helios. URL `https://nssdc.gsfc.nasa.gov/nmc/spacecraft/display.action?id=1974-097A`. viewed in : 15/08/2023.

[59] NASA web page, Pegasus. URL `https://nssdc.gsfc.nasa.gov/nmc/spacecraft/display.action?id=1965-009A`. viewed in : 15/08/2023.

[60] NASA web page, Pioneer 10. URL `https://nssdc.gsfc.nasa.gov/nmc/spacecraft/display.action?id=1972-012A`. viewed in : 15/08/2023.

[61] NASA web page, Solar Cycle Progression and Forecast. URL `https://www.nasa.gov/msfcsolar`. viewed in : 11/09/2023.

[62] NASA web page, Stardust. URL `https://nssdc.gsfc.nasa.gov/nmc/spacecraft/display.action?id=1999-003A`. viewed in : 15/08/2023.

[63] NOAA, NASA, and U. S. Air-Force. *U.S. Standard Atmosphere, 1976.* 1976. URL `https://ntrs.nasa.gov/api/citations/19770009539/downloads/19770009539.pdf`.

[64] F. Odom, G. Richter, J. Brown, B. Martinsen, R. Cai, M. Fellows, A. Wolf, C. Montag, P. Young, J. A. Carmona-Reyes, J. Schmoke, M. Cook, B. Garner, I. Gravagne, K. Pin, L. Shedd, T. Groskreutz, T. Hegle, N. Mulenos, J. Stone, C. Wiley, V. Yanga, D. Eustice, K. Flachsbart, N. Steele, C. Tilley, P. Friudenberg, D. Penshorn, L. Henderson, E. Cavazos, A. Nabili, E. Cox, A. Cox, J. Wood, L. Devine, J. Curran, A. Mendiola, C. Falkner, R. Laufer, R. Srama, K. E. Schubert, L. S. Matthews, G. Light-Sey, and T. W. Hyde. Piezoelectric dust detector design and calibration for the armadillo. *46th Lunar and planetary Science Conference, Woodlands (Texas)*, 2015. URL `https://www.hou.usra.edu/meetings/lpsc2015/pdf/2191.pdf`.

[65] F. Scala, M. Trisolini, and C. Colombo. Attitude control of the disposal phase of the ecube mission for the atmospheric data acquisition. *16th International conference on Space operations, Cape Town (South Africa)*, 2021.

[66] J. P. Schwanethal, N. Mcbride, S. F. Green, J. A. M. Mcdonnell, and G. Drolshagen. Analysis of impact data from the debie (debris in-orbit evaluator) sensor in polar low earth orbit. *4th European Conference on Space Debris ESA SP-587, Darmstadt (Germany)*, 2005.

[67] T. H. See, M. K. Allbrooks, D. R. Atkinson, C. A. Sapp, C. G. Simon, and M. E. Zolensky. Meteoroid debris special investigation group data acquisition procedures. 1995. URL `https://www.researchgate.net/publication/2700999_Meteoroid_Debris_Special_Investigation_Group_Data_Acquisition_Procedures`.

[68] Space-Track catalogue. URL `https://www.space-track.org/`.

[69] Space Wether Prediction Senter - NOAA, Solar Cycle Progression. URL `https://www.swpc.noaa.gov/products/solar-cycle-progression`. viewed in : 11/09/2023.

[70] A. J. Tuzzolino. Applications of pvdf dust sensor systems in space. *Advances in Space Research*, 17:123–132, 1996. doi: 10.1016/0273-1177(95)00769-B.

[71] A. J. Tuzzolino, R. B. Mckibben, J. A. Simpson, S. Benzvi, H. D. Voss, and H. Gursky. The space dust (spadus) instrument aboard the earth-orbiting argos spacecraft: I-instrument description. *Planetary and Space Science*, 49:689–703, 2001. URL `www.elsevier.nl/locate/planspasci`.

[72] A. J. Tuzzolino, T. E. Economou, R. B. McKibben, J. A. Simpson, S. Benzvi, L. Blackburn, H. D. Voss, and H. Gursky. Final results from the space dust (spadus) instrument flown aboard the earth-orbiting argos spacecraft. *Planetary and Space Science*, 53:903–923, 7 2005. ISSN 00320633. doi: 10.1016/j.pss.2005.03.008.

[73] M. Uetsuhara, M. Okada, Y. Yamazaki, and A. P. L. T. Hanada. Sub-millimeter size debris monitoring system with idea osg 1. *Advanced Maui Optical and Space Surveillance Technologies Conference (AMOS)*, 2016. URL `www.amostech.com`.

[74] D. A. Vallado. *Fundamentals of astrodynamics and applications*. McGraw-Hill, 1997. Table 7-4 , pag.510.

A | **Appendix A**

Mission	Launch	Status	Environment	Orbit	Instrument	Detection Method
Explorer 13	1961	Fail orbit	Earth	-	-	- MOS - Pressurized penetration - PZT
Explorer 16	1962	Decayed	Earth	750 x 1181 km, i=52°	-	- MOS - Pressurized penetration - PZT
Pegasus	1965	Decayed	Earth	-	-	MOS
Pioneer 8-9	1967-68	-	Sun	-	-	Impact ionization
Explorer 46	1972	Decayed	Earth	496 x 814 km, i=37.7°	-	- MOS - Pressurized penetration
Pioneer 10	1972	-	Jupiter/outer space	-		Pressurized penetration
Helios	1974	-	Sun	-		Impact ionization
SJ 2	1981	Decayed	Earth	232 x 1598 km, i=59°	IP	-
LDEF	1984	Retrived	Earth			

Mission	Launch	Status	Environment	Orbit	Instrument	Detection Method
Giotto	1985	-	Halley comet	-	DIDSY	- PZT - Ionization Impact
Galileo	1989	Decayed	Jupiter	-	DDS	Impact ionization
Ulysses	1990	-	Sun	-	DUST	Impact ionization
EURECA	1992	Retrieved	Earth			
Cassini	1997	Decayed	Saturn	-	CDA	Impact ionization
Nozomi	1998	Fail	Mars	-		Impact ionization
ARGOS	1999	-	Earth	Circular, 850 km , SSO	SPADUS	PVDF
Stardust	1999	-	comet P/Wild2	-	CIDA & DFMI	- Impact ionization - PVDF
Proba 1	2001	-	Earth	543 x 657 km, i=97.9°	DEBIE	- Impact ionization - PZT
Rosetta	2004	-	Comet 67P	-	GIADA	- Optical fence - PZT
New Horizons	2006	-	Pluto	-	SDC	PVDF
AIM	2007	-	Earth	Circular, 600 km , SSO	CDE	PVDF

Mission	Launch	Status	Environment	Orbit	Instrument	Detection Method
Kagayaki	2009	-	Earth	Circular, 600 km , SSO	MOIS	Sail and camera
Ikaros	2010	-	Inner planet	-	ALADDIN	
Idea OSG 1	2017	Launch fail	Earth	600 x 800 km , i=98°	SDM	Electric strips on non conductive film
ISS (Dragons)	2017	-	Earth	400 x 423 km, i=51.65°	SDS DRAGONS	• thin film • electric grid • PZT
BepiColombo	2018	-	Mercury	-	MDM	PZT
Armadillo	2019	Decayed	Earth	305 x 851 km , i=28.54°	PDD	• Impact ionization • PZT
Asterisc	2021	-	Earth	Circular, 560 km , SSO	-	thin film with PZT
SJ 21	2021	-	Earth	-	-	
Milani CubeSat	2024	-	Dydimos	-	VISTA	-

Table A.1: Debris and Dust detection : Past missions [13][49][68].

Instrument		Mass	Dimension	Power	Data Rate	Detection Area	mass range		diameter range
		[kg]	[mm]	[W]	[kbit/s]	[m^2]	[g]		[μm]
DDS		4.2	-	5.4	0.024	0.1	1e-16 to 1e-6		-
CDA		16.36	810x670x450	18	0.524	0.1	1.3e-16 to 1.2e-4		-
SPADUS		23.4	-	6.3	-	0.058	5e-12 to 1e-5		2 to 200
CIDA		-	-	-	-	0.011	-		-
DEBIE	SU	0.56	100x100x47	4	-	0.01 x #SU	5e-14 to 1e-7		-
	DPU	0.74	156x136x42.5						
ISIS		-	-	-	-	s/c surface	-		1 to 100
GIADA	GDS	5.90	-	-	-	0.01	-		60 to 1e3
	IS					0.01	6.5e-10 to 4e-4 $kg*m/s$		
MDD		1.3	360x250x28	-	-	0.1	-		-
SDC		1.9	450x300	5	-	0.11	1e-12 to 5e-9		-
CDE		-	-	-	-	0.1	1e-11 to 5e-9		0.8 to 8
Horyu-II detector		0.023	90x90	-	-	0.0022	-		100 to 600
SDM (IdeaOSG1)		-	-	-	-	0.1	-		100 to 1e3
MDM		0.6	-	4	-	0.0064	1e-14 to 1e-8		-
PDD (Armadillo)		0.4	80x80x40	3	150 kByte/day	0.0040	-		1 to 1e3
SCODD		-	200x200x193	-	-	0.04	-		-

Table A.2: Dust detection Instrument.